Theoret.Appl.Mech. TEOPM7, Vol.41, No.4, pp. 283–322, Belgrade 2014 *

THE DARCY-FORCHHEIMER LAW FOR MODELLING FLUID FLOW IN BIOLOGICAL TISSUES

Alfio Grillo **Melania Carfagna** **Salvatore Federico**

*doi:10.2298/TAM1404281G Math.Subj.Class.: 74B20, 74D10, 74E05, 74E10, 74E30, 74F10.

According to: *Tib Journal Abbreviations (C) Mathematical Reviews*, the abbreviation TEOPM7 stands for TEORIJSKA I PRIMENJENA MEHANIKA.

Theoret. Appl. Mech., Vol.41, No.4, pp. 283–322, Belgrade 2014

The Darcy-Forchheimer law for modelling fluid flow in biological tissues

Alfio Grillo* **Melania Carfagna†** **Salvatore Federico‡**

Abstract

The motion of the interstitial fluid of a biological tissue is studied by employing the Darcy-Forchheimer law, a correction to standard Darcy's law. The tissue is modelled as a saturated biphasic medium comprising the fluid and a deformable matrix. The reason for undertaking this study is that a description of the tissue's dynamics based on the Darcy-Forchheimer law might be more complete than the one based on Darcy's law, since the former provides a better macroscopic representation of the microscopic fluid-solid interactions. Through numerical simulations, we analyse the influence of the Forchheimer's correction.

Keywords: Biological Tissues, Porous Media, Darcy-Forchheimer Law.

1 Introduction

From the point of view of Mechanics, articular cartilage can be classified as a fibre-reinforced, composite material in which two principal constituents can be distinguished: an interstitial fluid, mainly consisting of water, and a matrix of proteoglycans, reinforced by collagen fibres [45]. The composition of articular cartilage, as well as the distribution and orientation of the collagen fibres, vary from the upper to the lower strata of the tissue [46, 50],

*Corresponding Author. DISMA "G. L. Lagrange", Politecnico di Torino, Torino, Italy. E-mail: alfio.grillo@polito.it

†DISMA "G. L. Lagrange", Politecnico di Torino, Torino, Italy. E-mail: melania.carfagna@polito.it

‡Dept of Mechanical and Manufacturing Engineering, The University of Calgary, Calgary, Canada Email: salvatore.federico@ucalgary.ca

thereby rendering its mechanical properties inhomogeneous and anisotropic. Also the ease with which the fluid moves through the matrix —a property measured by the tissue's permeability— is affected by the tissue's inhomogeneity and anisotropy. The influence wielded by the collagen fibres on the flow properties of the overall tissue was suggested by Maroudas and Bullough [46] on the basis of experimental evidences, and has been recently investigated, e.g., in [18, 19].

The motion of the interstitial fluid of articular cartilage is tightly connected with the stresses and deformations that can be generated in the tissue [43]. The Theory of Mixtures, formulated for solid-fluid biphasic materials [9,33,53], offers a quite natural theoretical framework for studying, at the tissue scale, the coupling between the interstitial fluid and the solid constituents of articular cartilage. In this context, the solid phase can be studied either as a single-constituent material [36] or as a mixture of solids [6, 40]. Moreover, the solid phase is usually assumed to be incompressible and elastic (or hyperelastic), and the fluid phase is assumed to be incompressible and macroscopically inviscid.

Within the biphasic models of articular cartilage, the interplay between the motions of the fluid and the solid phase is usually described constitutively by introducing a deformation-dependent tissue's permeability [7, 36]. In the isotropic models, this transport property is expressed as a function depending solely on the deformation of the solid phase [36]. In the anisotropic models, instead, the statistical orientation of the collagen fibres is often accounted for [4,5,30,49], and the evolution of the tissue's anisotropy is put in relation with the variation of the tissue's deformation. These studies, originally developed in small deformations, have been recently reformulated in a finite-deformation setting, e.g., in [17], and implemented in Finite Element software in [52,59]. To this end, generalisations to some hyperelastic models of monophasic materials (cf., e.g., [15,37,48]) have been elaborated to allow for statistically oriented collagen fibres [17, 20, 59].

The model of articular cartilage that we present hereafter is far from being all-embracing. Rather, it is a simplified model, which does not account for the tissue's anisotropy. We follow this path in order to generalise one targeted aspect of the standard biphasic models which we are aware of. Indeed, a common feature of these models is the employment of Darcy's Law to describe the motion of the interstitial fluid. This choice is justified because the fluid phase moves slowly enough. Some authors, instead, on the basis of an extended Hamilton-Rayleigh Principle, consider friction and

inertial effects and a proper set of boundary conditions at "fluid-permeable interfaces between dissimilar fluid-filled porous matrices" that are "relative to volume Darcy-Brinkman and to surface Saffman-Beavers-Joseph dissipation effects" [14].

In this paper, however, we propose to describe the fluid flow by means of the so-called Darcy-Forchheimer equation [60]. This is a correction to the standard Darcy's Law, which consists of introducing a non-linear relationship between the filtration velocity and the pressure gradient. We adhere to this modelling choice with the goal of investigating how the switch from a linear to a non-linear model of the flow can lead to changes in the overall mechanical response of the whole solid-fluid system. To our knowledge, in the framework of the Biomechanics of articular cartilage, the Forchheimer's correction was mentioned in [41], although both the model and the simulations were performed by means of standard Darcy's Law.

Many theoretical studies have been performed to motivate the experimental evidence of the Darcy-Forchheimer law [34, 56, 60]. In fact, the Forchheimer's correction can be related to the surface integrals of the contact forces exchanged between the fluid and the solid phase at the pore scale [10, 32, 60]. These integrals, which are computed over the solid-fluid interface, involve the overall Cauchy stress tensor of the fluid phase and, partially, the contribution given by the pore scale fluctuations of the fluid velocity. Thus, both the pore scale inertial effects and the solid-fluid interactions, which become larger when the filtration velocity increases, seem to be possible contributory causes to the non-linearity of the Forchheimer's correction.

2 Mass and momentum balance laws

The biphasic system considered in this paper constitutes the simplest representation of hydrated biological tissue, in which the solid phase describes the tissue's porous matrix and the fluid phase models the biological fluid occupying the pores of the matrix. In the following, the fluid phase is also referred to as interstitial fluid. The theory elaborated hereafter rests on the fundamental hypothesis that the biphasic system is saturated. This means that the pore space of the system is entirely filled with the fluid phase.

We refer to the kinematics of biphasic mixtures put forward in [44, 54, 55], and recently adopted in [59] for soft biological tissues. We denote by $\mathcal{C}_t$ and $\mathcal{C}_\mathrm{R}$ the subsets of the three-dimensional Euclidean point space $\mathcal{S}$

corresponding to the current configuration and the reference configuration of the mixture, respectively. Here, t denotes a generic instant of time. The motion of the solid is represented by the one-parameter family of smooth mappings $\chi(\,\cdot\,,t) : \mathcal{C}_\mathrm{R} \to \mathcal{S}$, such that $x = \chi(X,t) \in \mathcal{S}$, with $X \in \mathcal{C}_\mathrm{R}$. At each spatial point $x \in \mathcal{C}_t$, the solid and the fluid phase co-exist.

The deformation gradient tensor of the solid phase is denoted by $\boldsymbol{F}$, and the right Cauchy-Green deformation tensor by $\boldsymbol{C} = \boldsymbol{F}^\mathrm{T}.\boldsymbol{F} = \boldsymbol{F}^\mathrm{T}\boldsymbol{g}\boldsymbol{F}$, with $\boldsymbol{g}$ being the spatial metric tensor (see [47] for details). In order for χ to be admissible, the volumetric ratio $J := \det(\boldsymbol{F})$ must be positive at all $X \in \mathcal{C}_\mathrm{R}$ and at all times. Given the systems of coordinates $\{\hat{x}^a\}_{a=1}^3$ and $\{\hat{X}^A\}_{A=1}^3$, associated with $\mathcal{C}_t$ and $\mathcal{C}_\mathrm{R}$, respectively, the tensor components of $\boldsymbol{F}$ and $\boldsymbol{C}$ read $F^a{}_A = \partial\chi^a/\partial X^A$ and $C_{AB} = F^a{}_A g_{ab} F^b{}_B$, with g_{ab} being the components of $\boldsymbol{g}$. The velocities of the solid and fluid particle passing through $x = \chi(X,t)$ at time t are given by $\boldsymbol{v}_\mathrm{s}(x,t) = \dot{\chi}(X,t)$ and $\boldsymbol{v}_\mathrm{f}(x,t)$, respectively, where the superimposed dot means partial differentiation with respect to time. Finally, we also introduce the relative velocity $\boldsymbol{v}_\mathrm{fs} = \boldsymbol{v}_\mathrm{f} - \boldsymbol{v}_\mathrm{s}$.

We consider a simplified framework in which no mass exchanges between the solid and the fluid phase are accounted for. Moreover, we assume that the macroscopic inertial forces and the external body forces (such as gravity) acting on the mixture are negligible. These hypotheses, which are commonly accepted in the biomechanical models of soft tissues, lead to the following set of equations, which represent the local form of the balance laws of mass and linear momentum for the solid and fluid phase of the mixture:

$$\partial_t(\phi_\mathrm{s}\varrho_\mathrm{s}) + \mathrm{div}(\phi_\mathrm{s}\varrho_\mathrm{s}\boldsymbol{v}_\mathrm{s}) = 0\,, \tag{1a}$$

$$\partial_t(\phi_\mathrm{f}\varrho_\mathrm{f}) + \mathrm{div}(\phi_\mathrm{f}\varrho_\mathrm{f}\boldsymbol{v}_\mathrm{f}) = 0\,, \tag{1b}$$

$$\mathrm{div}(\boldsymbol{\sigma}_\mathrm{s}) + \boldsymbol{m}_\mathrm{s} = \boldsymbol{0}\,, \tag{1c}$$

$$\mathrm{div}(\boldsymbol{\sigma}_\mathrm{f}) + \boldsymbol{m}_\mathrm{f} = \boldsymbol{0}\,, \tag{1d}$$

$$\boldsymbol{m}_\mathrm{s} + \boldsymbol{m}_\mathrm{f} = \boldsymbol{0}\,. \tag{1e}$$

The product $\phi_\alpha\varrho_\alpha$ ($\alpha = \mathrm{s},\mathrm{f}$) is the apparent density of the αth phase. It depends on the true mass density ϱ_α and the volumetric fraction ϕ_α, which describes the volumetric content of the αth phase in a representative volume element of the mixture. The second-order tensor $\boldsymbol{\sigma}_\alpha$ ($\alpha = \mathrm{s},\mathrm{f}$) represents the Cauchy stress tensor of the αth phase, and $\boldsymbol{m}_\alpha$ is the rate at which the αth phase exchanges linear momentum with the other one. Finally, the closure condition (1e) states that linear momentum is neither produced nor destroyed by the mixture as a whole. The mixture is thus said to be "closed" with respect to momentum.

From here on, we assume that ϱ_{s} and ϱ_{f} are given constants (this assumption implies the intrinsic incompressibility of both the solid and the fluid phase). Moreover, we require the saturation constraint $\phi_{\mathrm{s}} + \phi_{\mathrm{f}} = 1$, which has to apply at all points of the mixture and at all times, and invoke (1e) to rewrite (1a)–(1d) in the following equivalent form:

$$D_{\mathrm{s}}\phi_{\mathrm{s}} + \phi_{\mathrm{s}} \operatorname{div} \boldsymbol{v}_{\mathrm{s}} = 0\,, \tag{2a}$$

$$\operatorname{div} \boldsymbol{v}_{\mathrm{s}} + \operatorname{div} \boldsymbol{q} = 0\,, \tag{2b}$$

$$\operatorname{div}(\boldsymbol{\sigma}_{\mathrm{s}} + \boldsymbol{\sigma}_{\mathrm{f}}) = \boldsymbol{0}\,, \tag{2c}$$

$$\operatorname{div}(\boldsymbol{\sigma}_{\mathrm{f}}) + \boldsymbol{m}_{\mathrm{f}} = \boldsymbol{0}\,. \tag{2d}$$

In (2a), $D_{\mathrm{s}}\phi_{\mathrm{s}} = \partial_t \phi_{\mathrm{s}} + (\operatorname{grad} \phi_{\mathrm{s}})\boldsymbol{v}_{\mathrm{s}}$ is the substantial derivative of ϕ_{s} computed with respect to the solid motion and, in (2b), $\boldsymbol{q} = \phi_{\mathrm{f}} \boldsymbol{v}_{\mathrm{fs}}$ is said to be the *filtration velocity*.

3 Constitutive theory and dissipation

We assume that the solid phase can be modelled as a hyperelastic material from the reference configuration $\mathcal{C}_{\mathrm{R}}$, which is regarded as unloaded and stress-free, and that the fluid phase is macroscopically inviscid. Accordingly, it can be proven that the Cauchy stress tensors $\boldsymbol{\sigma}_{\mathrm{s}}$ and $\boldsymbol{\sigma}_{\mathrm{f}}$ are given by [9, 17, 24, 33]

$$\boldsymbol{\sigma}_{\mathrm{s}} = -\phi_{\mathrm{s}} p\, \boldsymbol{g}^{-1} + \boldsymbol{\sigma}_{\mathrm{sc}}\,, \qquad \boldsymbol{\sigma}_{\mathrm{sc}} = \frac{1}{J}\, \boldsymbol{F} \left(2 \frac{\partial \hat{W}}{\partial \boldsymbol{C}}(\boldsymbol{C}) \right) \boldsymbol{F}^{\mathrm{T}}\,, \tag{3a}$$

$$\boldsymbol{\sigma}_{\mathrm{f}} = -\phi_{\mathrm{f}} p\, \boldsymbol{g}^{-1}\,, \tag{3b}$$

where p is pressure, $\boldsymbol{\sigma}_{\mathrm{sc}}$ is the constitutive part of the solid phase Cauchy stress tensor, and $\hat{W}$ is the strain energy density function of the solid phase measured per unit volume of $\mathcal{C}_{\mathrm{R}}$. Because of the hypothesis of incompressibility of the solid and fluid phase, p has to be understood as a Lagrange multiplier. Moreover, consistently with the assumption of inviscid fluid, the Cauchy stress tensor $\boldsymbol{\sigma}_{\mathrm{f}}$ is purely hydrostatic. Finally, by exploiting the results (3a) and (3b), we can rewrite (2c) and (2d) as

$$\operatorname{div}(-p\, \boldsymbol{g}^{-1} + \boldsymbol{\sigma}_{\mathrm{sc}}) = \boldsymbol{0}\,, \tag{4a}$$

$$-\phi_{\mathrm{f}} \boldsymbol{g}^{-1} \operatorname{grad} p + \left(\boldsymbol{m}_{\mathrm{f}} - p \boldsymbol{g}^{-1} \operatorname{grad} \phi_{\mathrm{f}} \right) = \boldsymbol{0}\,. \tag{4b}$$

By Piola-transforming (2a) with respect to the solid phase motion, and employing the identity $\dot{J} = J \operatorname{div} \boldsymbol{v}_{\mathrm{s}}$, the mass balance law of the solid phase reads

$$\dot{\overline{J\phi_{\mathrm{s}}}} = 0\,. \tag{5}$$

From (5), we can state that $\phi_{\mathrm{sR}} := J\phi_{\mathrm{s}}$, which is the Piola transformation of ϕ_{s}, is independent of time. From a physical point of view, ϕ_{sR} measures the volumetric content of the solid phase in a representative volume of the reference configuration $\mathcal{C}_{\mathrm{R}}$. For this reason, it is also referred to as "referential volumetric fraction" of the solid phase.

In general, ϕ_{sR} is a function of the points $X \in \mathcal{C}_{\mathrm{R}}$. If ϕ_{sR} is known, then ϕ_{s} can be univocally determined as a function of the volumetric ratio J, i.e.

$$\phi_{\mathrm{s}} = \frac{\phi_{\mathrm{sR}}}{J}. \tag{6}$$

The remaining equations (2b), (4a) and (4b) constitute a set of seven scalar equations in the ten unknowns χ, $\boldsymbol{q}$, p, and $\boldsymbol{m}_{\mathrm{f}}$. The stress tensor $\boldsymbol{\sigma}_{\mathrm{sc}}$ is not regarded as unknown, since it is prescribed constitutively in (3a). Here, we postulate that $\hat{W}(\boldsymbol{C})$ is of the Holmes-Mow type [36], i.e.

$$\hat{W}(\boldsymbol{C}) = \alpha_0 \left([\hat{I}_3(\boldsymbol{C})]^{-b} \mathrm{e}^{\left[\alpha_1(\hat{I}_1(\boldsymbol{C})-3)+\alpha_2(\hat{I}_2(\boldsymbol{C})-3)\right]} - 1 \right) . \tag{7}$$

In (7), α_0 is a measure of the stiffness of the solid phase, α_1, α_2 and b are model parameters satisfying the condition $\alpha_1 + 2\alpha_2 = b$, and $\hat{I}_1$, $\hat{I}_2$ and $\hat{I}_3$ are the invariants of $\boldsymbol{C}$:

$$I_1 = \hat{I}_1(\boldsymbol{C}) = \operatorname{tr}(\boldsymbol{C})\,, \tag{8a}$$

$$I_2 = \hat{I}_2(\boldsymbol{C}) = \tfrac{1}{2} \left\{ [\hat{I}_1(\boldsymbol{C})]^2 - \operatorname{tr}[\boldsymbol{C}.\boldsymbol{C}] \right\} , \tag{8b}$$

$$I_3 = \hat{I}_3(\boldsymbol{C}) = \det(\boldsymbol{C}) = J^2\,. \tag{8c}$$

In order to close the problem, we select χ, $\boldsymbol{q}$ and p as independent unknowns, and look for a constitutive law determining $\boldsymbol{m}_{\mathrm{f}}$. In this work, we deduce such a constitutive law from the Principle of Maximum Dissipation [31]. For this purpose, we introduce a dissipation function and maximise it over a suitable set of variables. For the considered biphasic system, and within a purely mechanical framework, the dissipation function reduces to

$$\mathfrak{D} := -\frac{1}{\phi_{\mathrm{f}}} \left\{ \boldsymbol{m}_{\mathrm{f}} - p\, \boldsymbol{g}^{-1} \mathrm{grad}\phi_{\mathrm{f}} \right\} . \boldsymbol{q} \geq 0\,, \tag{9}$$

where $\mathfrak{D}$ is defined per unit volume of the current configuration $\mathcal{C}_t$. Following [9, 33, 59], we rewrite $\boldsymbol{m}_{\mathrm{f}}$ as

$$\boldsymbol{m}_{\mathrm{f}} = \boldsymbol{m}_{\mathrm{fd}} + p\,\boldsymbol{g}^{-1}\mathrm{grad}\phi_{\mathrm{f}}\,, \tag{10}$$

where $\boldsymbol{m}_{\mathrm{fd}}$ and $p\,\boldsymbol{g}^{-1}\mathrm{grad}\phi_{\mathrm{f}}$ are said to be the dissipative and non-dissipative contributions to $\boldsymbol{m}_{\mathrm{f}}$, respectively. Hence, by substituting (10) into (9), we obtain

$$\mathfrak{D} = -\frac{1}{\phi_{\mathrm{f}}}\boldsymbol{m}_{\mathrm{fd}}.\boldsymbol{q} \geq 0\,, \tag{11}$$

and, by substituting (10) into (4b), the balance of momentum for the fluid phase becomes

$$\boldsymbol{m}_{\mathrm{fd}} = \phi_{\mathrm{f}}\boldsymbol{g}^{-1}\mathrm{grad}\,p\,. \tag{12}$$

We recall that, due to the saturation constraint, and using (6), ϕ_{f} can be written as $\phi_{\mathrm{f}} = 1 - \phi_{\mathrm{s}} = (J - \phi_{\mathrm{sR}})/J$. Moreover, by choosing $\boldsymbol{F}$ and $\boldsymbol{q}$ as the independent constitutive variables, we postulate a constitutive law of the type $\boldsymbol{m}_{\mathrm{fd}} = \hat{\boldsymbol{m}}_{\mathrm{fd}}(\boldsymbol{F}, \boldsymbol{q})$. Consistently, $\mathfrak{D}$ can be rewritten as a constitutive function of the same set of variables, i.e.

$$\mathfrak{D} = \hat{\mathfrak{D}}(\boldsymbol{F}, \boldsymbol{q}) = -\frac{J}{J - \phi_{\mathrm{sR}}}\hat{\boldsymbol{m}}_{\mathrm{fd}}(\boldsymbol{F}, \boldsymbol{q}).\boldsymbol{q} \geq 0\,. \tag{13}$$

3.1 Darcy-Forchheimer law

In several problems of engineering relevance, $\hat{\boldsymbol{m}}_{\mathrm{fd}}$ is assumed to depend linearly on $\boldsymbol{q}$ (cf., e.g., [8]), i.e.,

$$\boldsymbol{m}_{\mathrm{fd}} = \hat{\boldsymbol{m}}_{\mathrm{fd}}(\boldsymbol{F}, \boldsymbol{q}) = -\boldsymbol{g}^{-1}\,\hat{\boldsymbol{r}}(\boldsymbol{F})\,\boldsymbol{q}\,, \tag{14}$$

where $\boldsymbol{r} = \hat{\boldsymbol{r}}(\boldsymbol{F})$ is a second-order tensor representing the resistivity of the porous medium to fluid flow (cf., e.g., [33]). By substituting (14) into (12), and solving for $\boldsymbol{q}$, we obtain Darcy's Law, i.e.

$$\boldsymbol{q} \equiv \boldsymbol{q}_{\mathrm{D}} = -\boldsymbol{k}\,\mathrm{grad}\,p\,, \tag{15}$$

where the subscript "D" means that the filtration velocity is computed according to Darcy's Law, and $\boldsymbol{k} = \hat{\boldsymbol{k}}(\boldsymbol{F})$ is the *hydraulic conductivity* of the porous medium. In this work, both $\boldsymbol{r}$ and $\boldsymbol{k}$ are assumed to be symmetric and positive definite, and it holds that $\boldsymbol{k} = \phi_{\mathrm{f}}\,\boldsymbol{r}^{-1}$. Moreover, $\hat{\boldsymbol{m}}_{\mathrm{fd}}(\boldsymbol{F}, \boldsymbol{q}_{\mathrm{D}})$ vanishes if, and only if, $\boldsymbol{q}_{\mathrm{D}}$ is null. By substituting (14) into (11), we obtain

$$\mathfrak{D} = \mathfrak{D}_{\mathrm{Darcy}} = \frac{1}{\phi_{\mathrm{f}}}\,\mathrm{sym}(\boldsymbol{r}) : (\boldsymbol{q}_{\mathrm{D}} \otimes \boldsymbol{q}_{\mathrm{D}}) \geq 0\,. \tag{16}$$

The Piola transformation of $\boldsymbol{q}_{\mathrm{D}}$ determines the material form of Darcy's law:

$$\boldsymbol{Q}_{\mathrm{D}} := J\boldsymbol{F}^{-1}\boldsymbol{q}_{\mathrm{D}} = -\boldsymbol{K}\mathrm{Grad}\, p\,, \tag{17}$$

with $\boldsymbol{K} = J\boldsymbol{F}^{-1}\boldsymbol{k}\boldsymbol{F}^{-\mathrm{T}}$ being the material hydraulic conductivity tensor, i.e. the Piola transform of $\boldsymbol{k}$ with respect to the solid motion. We notice that, since $\boldsymbol{K}$ can be expressed constitutively as $\boldsymbol{K} = \hat{\boldsymbol{K}}(\boldsymbol{F})$, $\boldsymbol{Q}_{\mathrm{D}}$ can be written as:

$$\boldsymbol{Q}_{\mathrm{D}} = \hat{\boldsymbol{Q}}_{\mathrm{D}}\left(\boldsymbol{F}, \boldsymbol{H}\right)\,, \tag{18}$$

where $\boldsymbol{H} := \mathrm{Grad}\, p$ is the material pressure gradient.

Here, however, we adhere to a different constitutive framework, which is based on the assumption [10,35]

$$\boldsymbol{m}_{\mathrm{fd}} = \hat{\boldsymbol{m}}_{\mathrm{fd}}(\boldsymbol{F}, \boldsymbol{q}) = -\left(1 + \hat{A}(\boldsymbol{F})\|\boldsymbol{q}\|\right)\boldsymbol{g}^{-1}\hat{\boldsymbol{r}}(\boldsymbol{F})\boldsymbol{q}\,. \tag{19}$$

The positive-definite quantity $A = \hat{A}(\boldsymbol{F})$ is referred to as *Forchheimer coefficient* (its physical units are $[A] = \mathrm{s/m}$). By substituting the right-hand-side of (19) into (12), and using the relation $\phi_{\mathrm{f}}\,\boldsymbol{r}^{-1} = \boldsymbol{k}$, we obtain

$$(1 + A\|\boldsymbol{q}\|)\boldsymbol{q} = -\boldsymbol{k}\,\mathrm{grad}\, p \equiv \boldsymbol{q}_{\mathrm{D}}\,. \tag{20}$$

A direct implication of this result is that the Euclidean norms of $\boldsymbol{q}_{\mathrm{D}}$ and $\boldsymbol{q}$ are related by the equality

$$(1 + A\|\boldsymbol{q}\|)\|\boldsymbol{q}\| = \|\boldsymbol{q}_{\mathrm{D}}\|\,, \tag{21}$$

which leads to the following second-order polynomial equation in $\|\boldsymbol{q}\|$:

$$A\|\boldsymbol{q}\|^2 + \|\boldsymbol{q}\| - \|\boldsymbol{q}_{\mathrm{D}}\| = 0\,. \tag{22}$$

Since the discriminant of (22) is strictly positive, it admits two real, distinct solutions. However, the only admissible solution, since it is the positive one, is given by

$$\|\boldsymbol{q}\| = \frac{-1 + \sqrt{1 + 4A\|\boldsymbol{q}_{\mathrm{D}}\|}}{2A}\,. \tag{23}$$

This result allows to write $\boldsymbol{q}$ explicitly as a function of $\boldsymbol{q}_{\mathrm{D}}$. Indeed, by substituting the right-hand-side of (23) into (20), and solving for $\boldsymbol{q}$, we find [27]

$$\boldsymbol{q} = f\boldsymbol{q}_{\mathrm{D}}\,, \qquad f \equiv \bar{f}(A\|\boldsymbol{q}_{\mathrm{D}}\|) := \frac{2}{1 + \sqrt{1 + 4A\|\boldsymbol{q}_{\mathrm{D}}\|}}\,. \tag{24}$$

For all possible realisations of A and $\|\boldsymbol{q}_{\mathrm{D}}\|$, $\bar{f}(A\|\boldsymbol{q}_{\mathrm{D}}\|)$ is strictly positive and smaller than, or equal to, unity. In particular, it holds that $\bar{f}(0) = 1$, and $\bar{f}(A\|\boldsymbol{q}_{\mathrm{D}}\|) \sim 1 - A\|\boldsymbol{q}_{\mathrm{D}}\|$, when $A\|\boldsymbol{q}_{\mathrm{D}}\|$ tends towards zero. This behaviour allows to recover Darcy's Law for small values of the product $A\|\boldsymbol{q}_{\mathrm{D}}\|$. Finally, it holds that $\bar{f}(A\|\boldsymbol{q}_{\mathrm{D}}\|) \sim (A\|\boldsymbol{q}_{\mathrm{D}}\|)^{-1/2}$, when $A\|\boldsymbol{q}_{\mathrm{D}}\|$ tends towards infinity. Clearly, the latter limit is only performed to comprehend the asymptotic behaviour of f, since too large values of $\|\boldsymbol{q}_{\mathrm{D}}\|$ have no physical meaning (we recall, indeed, that Darcy's Law is valid only for slow fluid flow). Since it holds true that $0 < f \leq 1$, the magnitude of the filtration velocity computed by means of the Forchheimer's correction, $\|\boldsymbol{q}\|$, is always a proper fraction of $\|\boldsymbol{q}_{\mathrm{D}}\|$.

The Piola transform of $\boldsymbol{q}$ reads

$$\boldsymbol{Q} := J\boldsymbol{F}^{-1}\boldsymbol{q} = f\,\boldsymbol{Q}_{\mathrm{D}}, \qquad f = \bar{f}\left(AJ^{-1}\sqrt{\mathcal{I}_4}\right), \tag{25}$$

where we used the equality

$$\|\boldsymbol{q}_{\mathrm{D}}\| = J^{-1}\sqrt{\boldsymbol{C} : (\boldsymbol{Q}_{\mathrm{D}} \otimes \boldsymbol{Q}_{\mathrm{D}})} = J^{-1}\sqrt{\mathcal{I}_4}\,, \tag{26}$$

and we introduced the "invariant" $\mathcal{I}_4 := \boldsymbol{C} : (\boldsymbol{Q}_{\mathrm{D}} \otimes \boldsymbol{Q}_{\mathrm{D}})$, which couples the deformation of the matrix with the Darcy's filtration velocity. Here, $\mathcal{I}_4$ mimics the invariant $\boldsymbol{C} : (\boldsymbol{M} \otimes \boldsymbol{M})$, which, in anisotropic materials, accounts for the coupling between the deformation and the local direction of anisotropy, expressed by the unit vector $\boldsymbol{M}$ (see, e.g., [37]). The result (18) and the constitutive expression of A allow to rewrite f as

$$f = \bar{f}\left(AJ^{-1}\sqrt{\mathcal{I}_4}\right) = \hat{f}\,(\boldsymbol{F}, \boldsymbol{H})\,. \tag{27}$$

Therefore, looking at (17) and (27), $\boldsymbol{Q}$ can be re-defined as

$$\boldsymbol{Q} = \hat{\boldsymbol{Q}}\,(\boldsymbol{F}, \boldsymbol{H}) = -\hat{f}(\boldsymbol{F}, \boldsymbol{H})\hat{\boldsymbol{K}}(\boldsymbol{F})\boldsymbol{H}\,, \tag{28}$$

with $\boldsymbol{H} = \mathrm{Grad}\, p$. Although $\boldsymbol{Q}$ depends on the same list of variables as $\boldsymbol{Q}_{\mathrm{D}}$, the Darcy-Forchheimer filtration velocity $\boldsymbol{Q}$ is highly non-linear both in the motion and in the material pressure gradient $\boldsymbol{H}$, whereas $\boldsymbol{Q}_{\mathrm{D}}$ is linear in $\boldsymbol{H}$ by definition. A direct consequence of this result is that the Piola transformation of (2b) transforms the mass balance law for the mixture as a whole into a highly non-linear partial differential equation in the pressure, i.e.

$$\dot{J} + \mathrm{Div}\,\boldsymbol{Q} = 0\,, \quad \Rightarrow \quad \dot{J} - \mathrm{Div}\,[f\boldsymbol{K}\,\mathrm{Grad}\, p] = 0\,. \tag{29}$$

3.2 Hydraulic conductivity

In this work, we restrict our investigation to the case of a porous medium characterised by isotropic hydraulic behaviour. The simplest constitutive law of $\boldsymbol{k}$ complying with isotropy takes on the form [7]

$$\boldsymbol{k} = \hat{\boldsymbol{k}}(\boldsymbol{F}) = \hat{k}_0(J)\boldsymbol{g}^{-1}\,, \tag{30}$$

where the dependence on $\boldsymbol{F}$ is through the volumetric ratio J. Following the non-linear isotropic cartilage model by Holmes and Mow [36], the scalar hydraulic conductivity $\hat{k}_0$ (whose physical units are $[\hat{k}_0] = \mathrm{m}^4/(\mathrm{Ns})$) can be defined as

$$\hat{k}_0(J) = k_{0\mathrm{R}}\left(\frac{J-\phi_{\mathrm{sR}}}{1-\phi_{\mathrm{sR}}}\right)^{m_0}\exp\left[\frac{m_1}{2}(J^2-1)\right]\,, \tag{31}$$

with m_0 and m_1 being constant material parameters. In the absence of deformation, i.e. when $J=1$, the identity $\hat{k}_0(1) = k_{0\mathrm{R}}$ is obtained, which means that the referential conductivity, $k_{0\mathrm{R}}$, is retrieved. The latter must describe the hydraulic properties of a porous medium at rest, and for which the interactions with the fluid flowing throughout it do not lead to deformations of the solid phase.

Even though the assumption of isotropic hydraulic behaviour is maintained, there may be cases in which more general constitutive laws for $\hat{\boldsymbol{k}}$ are required. For instance, a slight generalisation of (30) could be

$$\boldsymbol{k} = k_0\boldsymbol{g}^{-1} + k_1\boldsymbol{b}\,, \tag{32}$$

where $\boldsymbol{b} = \boldsymbol{F}.\boldsymbol{F}^{\mathrm{T}}$ is the left Cauchy-Green deformation tensor, while k_0 and k_1 are scalar functions whose constitutive expressions depend on $\boldsymbol{F}$ through the invariants of $\boldsymbol{C}$ (or, equivalently, of $\boldsymbol{b}$).

3.3 Summary of the model equations

By introducing the first Piola-Kirchhoff stress tensors

$$\boldsymbol{P}_{\mathrm{s}} = J\boldsymbol{\sigma}_{\mathrm{s}}\boldsymbol{F}^{-\mathrm{T}} = -\phi_{\mathrm{sR}}p\,\boldsymbol{g}^{-1}\boldsymbol{F}^{-\mathrm{T}} + \boldsymbol{P}_{\mathrm{sc}}\,, \tag{33a}$$

$$\boldsymbol{P}_{\mathrm{f}} = J\boldsymbol{\sigma}_{\mathrm{f}}\boldsymbol{F}^{-\mathrm{T}} = -(J-\phi_{\mathrm{sR}})p\,\boldsymbol{g}^{-1}\boldsymbol{F}^{-\mathrm{T}}\,, \tag{33b}$$

with $\boldsymbol{P}_{\mathrm{sc}} = J\boldsymbol{\sigma}_{\mathrm{sc}}\boldsymbol{F}^{-\mathrm{T}}$, the backward Piola-transformation of (4a) leads to

$$\mathrm{Div}\left(-Jp\,\boldsymbol{g}^{-1}\boldsymbol{F}^{-\mathrm{T}} + \boldsymbol{P}_{\mathrm{sc}}\right) = \boldsymbol{0}\,. \tag{34}$$

The strain energy density function (7) allows to determine $\boldsymbol{P}_{\rm sc}$ as a function of $\boldsymbol{F}$, i.e. $\boldsymbol{P}_{\rm sc} = \hat{\boldsymbol{P}}_{\rm sc}(\boldsymbol{F})$. Therefore, the overall stress $\boldsymbol{P} := \boldsymbol{P}_{\rm s} + \boldsymbol{P}_{\rm f}$ is given by

$$\boldsymbol{P} = \hat{\boldsymbol{P}}(p, \boldsymbol{F}) = -Jp\,\boldsymbol{g}^{-1}\boldsymbol{F}^{-\rm T} + \hat{\boldsymbol{P}}_{\rm sc}(\boldsymbol{F}). \tag{35}$$

Finally, by virtue of the results (6) and (28), the model equations reduce to

$$\dot{J} - {\rm Div}(f\boldsymbol{K}{\rm Grad}\, p) = 0\,, \tag{36a}$$

$${\rm Div}\left(-Jp\,\boldsymbol{g}^{-1}\boldsymbol{F}^{-\rm T} + \boldsymbol{P}_{\rm sc}\right) = \boldsymbol{0}\,, \tag{36b}$$

which constitute a closed set of coupled and highly non-linear partial differential equations in the unknowns χ and p. We remark that the difference between the standard model, which is based on Darcy's Law, and the one elaborated in this paper consists of the presence of the function f multiplying $\boldsymbol{Q}_{\rm D}$ in (36a). Clearly, the standard model is retrieved in the limit $f \to 1$. In the following, f is referred to as the "friction factor". To supply a constitutive expression for f, it is necessary to assign constitutively the Forchheimer coefficient A.

4 Forchheimer's coefficient

In the literature of porous media of both hydrogeological and industrial relevance, the Forchheimer coefficient A is often determined for porous media that are at rest and undeformable. Moreover, homogeneity and isotropy are often assumed. Thus, $\boldsymbol{k}$ becomes $k_{0\rm R}\boldsymbol{g}^{-1}$, with $k_{0\rm R}$ being a constant referential conductivity, and A is defined by

$$A = \varrho_{\rm f}\beta k_{0\rm R}\,, \tag{37}$$

where β is a parameter evaluated experimentally (we recall that $\varrho_{\rm f}$, i.e. the intrinsic mass density of the fluid phase, is constant in the present theory). Since A represents the inverse of a characteristic filtration velocity, i.e. $[A] =$ s/m, the physical units of β must be $[\beta] = 1/$m, so that β defines the inverse of a characteristic length scale.

To account for formulations of $\boldsymbol{k}$ that do not necessarily reduce to the one given in (30), and to allow for the extension of the definition (37) to deformable, inhomogeneous and anisotropic porous media, we introduce the *equivalent scalar conductivity*

$$k_{\rm eq} = \sqrt{\tfrac{1}{3}{\rm tr}[\boldsymbol{k}.\boldsymbol{k}]} \equiv \tfrac{1}{\sqrt{3}}\|\boldsymbol{k}\|\,. \tag{38}$$

Hence, we rephrase (37) as

$$A = \varrho_{\mathrm{f}} \beta k_{\mathrm{eq}} \,. \tag{39}$$

The equivalent conductivity, k_{eq}, depends on the same list of arguments as $\boldsymbol{k}$. Thus, we may write $k_{\mathrm{eq}} = \hat{k}_{\mathrm{eq}}(\boldsymbol{F})$. Since, in this paper, (30) applies, k_{eq} equals $\hat{k}_0$.

There exist several models that relate the β-factor to peculiar properties of the porous medium [1, 13, 16, 21, 38, 39, 42, 51, 57, 58]. In the work by Thauvin and Mohanty [58], these properties are represented by the porosity, permeability, and tortuosity of the considered porous medium (we recall that the porosity is equal to ϕ_{f} in the case of saturated porous media). In general, permeability and tortuosity are second-order tensors. The former is a measure of the ease with which a fluid permeates the pore space of a given porous medium, while the latter describes macroscopically the geometry of the pore space (for a mathematical definition of tortuosity, see, e.g., [8]). More specifically, it accounts for the fact that the trajectories followed by the fluid particles, or by particles of substances transported by the fluid, deviate from straight lines because of the meandrous structure of the pore space. Since, in a deformable porous medium, tortuosity varies with deformation, it should be expressed constitutively. In this paper, however, since the medium is assumed to be isotropic, we regard it as a scalar parameter.

Usually, in the literature dedicated to fluid flow in porous media of hydrogeological or industrial interest, the hydraulic conductivity $\boldsymbol{k}$ of a given porous medium is written as the ratio between the permeability of the medium, $\boldsymbol{\kappa}$, and the viscosity of the fluid, μ [8]:

$$\boldsymbol{k} = \frac{\boldsymbol{\kappa}}{\mu} \,. \tag{40}$$

Since $\boldsymbol{\kappa}$ and μ represent, respectively, a property of the porous medium and a property of the fluid, they are independent of each other, and both are needed to determine the hydraulic conductivity, which, instead, is a property of the pair "porous medium *and* fluid". In the simple case of isotropic media such that $\boldsymbol{\kappa} = \kappa_0 \boldsymbol{g}^{-1}$, the factor β is usually written as a power law of the scalar permeability κ_0, ϕ_{f}, and scalar tortuosity τ, i.e.

$$\beta = \bar{\beta}(\kappa_0, \phi_{\mathrm{f}}, \tau) = c_0 \, \kappa_0^{c_1} \phi_{\mathrm{f}}^{c_2} \tau^{c_3} \,, \tag{41}$$

where c_0 is a real proportionality constant [58], and c_1, c_2 and c_3 are real numbers. In this formulation, $\bar{\beta}$ is independent of viscosity.

A rather different approach is followed in the characterisation of the flow properties of biological tissues. Indeed, to the best of our knowledge, in Biomechanics one usually calls "permeability of a tissue" the quantity that one would call "hydraulic conductivity" in the jargon of porous media, and the constitutive laws found in the literature typically define $\boldsymbol{k}$ as a single tissue property, without separating the contribution of the true permeability from that of the fluid viscosity. For example, in the Holmes-Mow model of "soft gels and hydrated connective tissues in ultrafiltration" [36], although the definition of the tissue's "apparent permeability" does take into account the fluid viscosity, the experimental values assigned to $\hat{k}_{0\mathrm{R}}$ (k_0 in the notation of [36]) refer to a single characteristic quantity, withholding information about the fluid viscosity. To our understanding, the main advantage of this formulation is that the constitutive laws for $\boldsymbol{k}$, which have to be consistent with the experiments performed on a given tissue, and with the biological fluid flowing throughout it, do not constrain $\boldsymbol{k}$ to be of the form (40), a relation obtained for Newtonian fluids [8], thereby allowing for more general fluid behaviours.

To define the Forchheimer coefficient A for a biological tissue, we need to know β. However, the only expressions of β which we are aware of are the power laws assigned in (41), which make use of κ_0. Since we have numerical values only for k_{eq}, we introduce the *effective permeability* $\kappa_{\mathrm{eff}} := k_{\mathrm{eq}}\mu$, and re-define the factor β as

$$\beta = \bar{\beta}(\kappa_{\mathrm{eff}}, \phi_{\mathrm{f}}, \tau) = \bar{\beta}(k_{\mathrm{eq}}\mu, \phi_{\mathrm{f}}, \tau) = c_0\,(k_{\mathrm{eq}}\mu)^{c_1}\phi_{\mathrm{f}}^{c_2}\tau^{c_3}\,. \tag{42}$$

In table 1, each empirical law of the factor β is formulated in terms of $\kappa_{\mathrm{eff}} = k_{\mathrm{eq}}\mu$. This is done to retrieve the formulation of Thauvin and Mohanty [58], in which all expressions of β were presented in terms of permeability.

We regard the viscosity μ and the tortuosity τ as constant model parameters. Thus, by noticing that k_{eq} depends on the same list of arguments as $\boldsymbol{k}$, we can rewrite $\beta = \hat{\beta}(\boldsymbol{F})$. Finally, if k_{eq} is associated with the hydraulic conductivity defined by (30) and (31), the constitutive law for β can be rephrased as $\beta = \hat{\beta}(J)$. Hence, since also the constitutive law for the Forchheimer coefficient, $\hat{A}$, depends on the same list of arguments as β, we can write $A = \hat{A}(J)$. In contrast with the expressions of β supplied in [58], which are usually defined for non-deformable porous media, we re-defined here β as a function of the volumetric ratio, J, in order to account for the variations of permeability and porosity driven by the deformation.

We remark that the introduction of tortuosity as a free parameter of the model follows from the use of the expression (41), which has been taken from [58]. In the following, however, we set $\tau = 1$. This modelling choice, which could be too restrictive in some cases, is chiefly motivated by our lack of information about physically sound values or expressions of τ for the problem at hand. Nevertheless, it could be partially justified by admitting that the equivalent conductivity k_{eq} already accounts for tortuosity in its own definition.

Table 1: Expressions of β taken, and adapted, from [12, 58]. The effective permeability κ_{eff} has units $[\kappa_{\text{eff}}] = \text{m}^2$ and the β-factor has units $[\beta] = \text{m}^{-1}$.

β-Factor	Reference
$\beta_{\text{TM}} = 2.6591 \cdot 10^{-6} (\kappa_{\text{eff}})^{-0.98} \left(\frac{J - \phi_{\text{sR}}}{J} \right)^{-0.29}$	Thauvin & Mohanty [58]
$\beta_{\text{J}} = 4.9659 \cdot 10^{-8} (\kappa_{\text{eff}})^{-1.55}$	Jones [39]
$\beta_{\text{E}} = 1.419 \cdot 10^{-2} (\kappa_{\text{eff}})^{-1/2} \left(\frac{J - \phi_{\text{sR}}}{J} \right)^{-11/2}$	Ergun [16]
$\beta_{\text{G}} = 1.581 \cdot 10^{-1} (\kappa_{\text{eff}})^{-1/2} \left(\frac{J - \phi_{\text{sR}}}{J} \right)^{-5.5}$	Geertsma [21]
$\beta_{\text{JK}} = 5.8737 \cdot 10^{-7} (\kappa_{\text{eff}})^{-5/4} \left(\frac{J - \phi_{\text{sR}}}{J} \right)^{-3/4}$	Janicek & Katz [38]
$\beta_{\text{P}} = 3.6899 \cdot 10^{-2} \cdot (\kappa_{\text{eff}})^{-1.176}$	Pascal et al. [51]
$\beta_{\text{T}} = 2.9956 \cdot 10^{-4} (\kappa_{\text{eff}})^{-1.2}$	Tek et al. [57]
$\beta_{\text{CH}} = 9.4324 \cdot 10^{-11} (\kappa_{\text{eff}})^{-1.88} \left(\frac{J - \phi_{\text{sR}}}{J} \right)^{-0.449}$	Coles & Hartman [13]
$\beta_{\text{Li}} = 1.1 \cdot 10^{-3} (\kappa_{\text{eff}})^{-1} \left(\frac{J - \phi_{\text{sR}}}{J} \right)^{-1}$	Li et al. [42]
$\beta_{\text{A}} = 3.7595 (\kappa_{\text{eff}})^{-0.85}$	Aminian et al. [1]

By varying c_0, c_1, c_2 and c_3, several expressions of β can be built. To accomplish this task, we refer to the study conducted by Thauvin and Mohanty [58]. In (42), we adopt the isotropic hydraulic conductivity specified in (30), which implies $k_{\text{eq}} = \hat{k}_0(J)$, with $\hat{k}_0(J)$ being defined in (31). In this calculation, we consider both the homogeneous case, in which $k_{0\text{R}}$ is a given constant, and the inhomogeneous case, in which $k_{0\text{R}}$ depends on X. Looking at table 1, we notice that, since the values taken by c_1 are always negative, β decreases with increasing κ_{eff}. Thus, for a given distribution of the volumetric ratio J, higher values of $k_{0\text{R}}$ lead to smaller β-factors.

5 The confined compression test

The Forchheimer's correction manifests itself through the friction factor f. To evaluate its influence on the hydraulic and mechanical response of a sample of articular cartilage, we compare the solution to (36a) and (36b) obtained for $0 < f \leq 1$ with the solution obtained within the Darcy's approximation, which is retrieved by setting $f = 1$ in (36a). This amounts to replace $\boldsymbol{Q} = f\boldsymbol{Q}_{\mathrm{D}}$ with the standard Darcy's filtration velocity $\boldsymbol{Q}_{\mathrm{D}}$. For our purposes, we consider the benchmark problem known as "confined compression test". This test is, among others, largely used in Biomechanics to characterise, both *in vitro* and *in silico*, the hydraulic and mechanical properties of articular cartilage. We chose this benchmark problem because of its particularly simple setting.

5.1 Benchmark description and specific form of deformation

A cylindrical sample of articular cartilage is inserted into a cylindrical compression chamber characterised by an impermeable and rigid lateral wall. The bottom of the chamber consists of a fixed, impermeable and rigid plate. At the top, the chamber is delimited by a rigid and permeable plate, which is free to glide along the axial direction of the chamber.

Since the upper plate is permeable, the fluid contained in the specimen is allowed to flow out of the chamber during compression, thereby permitting the deformation of the specimen itself. The permeability of the upper plate is an essential condition. Indeed, if the upper plate were impermeable, no deformation could occur, since both the solid and the fluid phase constituting the sample are regarded as intrinsically incompressible. Furthermore, since the lateral wall and the lower plate of the chamber are impermeable, fluid flow is allowed only along the axial direction.

The hypothesis of isotropic and homogeneous material, the geometry of the specimen, and the prescriptions on the boundaries of the chamber make the confined compression test an axial-symmetric problem. Consequently, by employing cylindrical coordinates for parameterising both $\mathcal{C}_{\mathrm{R}}$ and $\mathcal{C}_t$, the deformation χ and pressure p can be specified as follows:

$$r = \chi^r(R, \Theta, Z, t) = R \in [0, R_{\mathrm{c}}]\,, \tag{43a}$$

$$\vartheta = \chi^\vartheta(R, \Theta, Z, t) = \Theta \in [0, 2\pi)\,, \tag{43b}$$

$$z = \chi^z(R, \Theta, Z, t) \equiv \zeta(Z, t) \in [0, \ell(t)]\,,\ \forall Z \in [0, L]\,, \tag{43c}$$

$$p(R, \Theta, Z, t) \equiv \wp(Z, t)\,. \tag{43d}$$

In (43a)–(43c), $\{r, \vartheta, z\}$ and $\{R, \Theta, Z\}$ denote the radial, circumferential and axial coordinate of the parameterisations of $\mathcal{C}_t$ and $\mathcal{C}_{\mathrm{R}}$, respectively, R_{c} and L are the radius and height of the undeformed specimen, and $\ell(t)$ is the deformed height at time t. In (43c) and (43d), the axial component of deformation χ^z and pressure p are re-defined as functions depending solely on the axial coordinate Z and time t. Equations (43a)–(43d) lead to the following matrix representations of $\boldsymbol{F}$ and $\boldsymbol{C}$:

$$[\boldsymbol{F}]^a{}_A = \mathrm{diag}\{1, 1, \zeta'\} = \mathrm{diag}\{1, 1, J\}\,, \tag{44a}$$

$$[\boldsymbol{C}]_{AB} = \mathrm{diag}\{1, 1, (\zeta')^2\} = \mathrm{diag}\{1, 1, J^2\}\,, \tag{44b}$$

where ζ' is the partial derivative of ζ with respect to the axial coordinate Z, and the last equality in (44a) and (44b) follows from the identity $J = \det(\boldsymbol{F}) = \zeta'$. Accordingly, also the matrix representation of the constitutive part of the first Piola-Kirchhoff stress tensor of the solid phase, $\boldsymbol{P}_{\mathrm{sc}}$, is diagonal, and the only component entering the model equations is the axial one P_{sc}^{zZ}. Due to the choice of the strain energy density function in (7), P_{sc}^{zZ} is given by

$$P_{\mathrm{sc}}^{zZ} \equiv \hat{P}_{\mathrm{sc}}^{zZ}(J) = \frac{H_{\mathrm{m}}}{2}\frac{J^2-1}{J^{2b+1}}\exp\{b[J^2-1]\}\,, \tag{45}$$

where $H_{\mathrm{m}} = 4\alpha_0[\alpha_1 + 2\alpha_2] = 4\alpha_0 b$ is the tissue's aggregate axial modulus [36].

Furthermore, the only non-zero component of the material filtration velocity $\boldsymbol{Q}$ is the axial one, Q^Z. By using (28) and (30), and recalling that $\boldsymbol{K} = J\boldsymbol{F}^{-1}\boldsymbol{k}\boldsymbol{F}^{-\mathrm{T}} = Jk_0\boldsymbol{C}^{-1}$, we obtain

$$Q^Z = -\frac{f k_0}{J}\wp'\,, \tag{46}$$

where $k_0 = \hat{k}_0(J)$ is specified in (31), $\wp'$ is the partial derivative of the pressure $\wp$ with respect to the axial coordinate Z, and the friction factor f becomes

$$f \equiv \bar{f}(A\|\boldsymbol{q}_{\mathrm{D}}\|) = \hat{f}(J, \wp') = \frac{2}{1+\sqrt{1+4A\frac{k_0|\wp'|}{J}}}\,. \tag{47}$$

We remark that, due to the considered simple setting, the friction factor f depends on the absolute value of the material pressure gradient $\wp'$. Finally,

the model equations (36a) and (36b) become

$$\dot{J} = \frac{\partial}{\partial Z}\left(\frac{f k_0}{J}\frac{\partial \wp}{\partial Z}\right), \tag{48a}$$

$$\frac{\partial \wp}{\partial Z} = \frac{\partial P_{\mathrm{sc}}^{zZ}}{\partial Z}. \tag{48b}$$

5.2 Boundary conditions and loading history

In order to determine the unknowns ζ and $\wp$ that solve the model equations (48a) and (48b), appropriate boundary conditions must be imposed. The boundary $\partial\mathcal{C}_{\mathrm{R}}$ of the reference configuration of the specimen can be written as $\partial\mathcal{C}_{\mathrm{R}} = \Gamma_{\mathrm{L}} \cup \Gamma_{\mathrm{B}} \cup \Gamma_{\mathrm{T}}$. The surfaces Γ_{B} and Γ_{T}, determined by the equations $Z = 0$ and $Z = L$, are in contact with the bottom and the top plate, respectively, while Γ_{L} is in contact with the lateral wall of the compression chamber. In this paper, we perform the confined compression test in force control. Hence, we apply the following loading protocol to the upper plate of the experimental apparatus:

$$\mathfrak{f}(t) = \begin{cases} \mathfrak{f}_{\max}\frac{t}{T_{\mathrm{ramp}}}, & t \in [0, T_{\mathrm{ramp}}], \\ \mathfrak{f}_{\max}, & t \in (T_{\mathrm{ramp}}, T_{\mathrm{end}}], \end{cases} \tag{49}$$

where the applied load $\mathfrak{f}(t)$ grows linearly in time until $t = T_{\mathrm{ramp}}$, and is then held constant up to $t = T_{\mathrm{end}}$. The maximum $\mathfrak{f}_{\max}$, reached at the end of the linear ramp, is chosen to be $\mathfrak{f}_{\max} = \gamma g_0$, where $g_0 = 9.81\ \mathrm{m/s^2}$ is the gravity acceleration, and γ is a proportionality constant having physical units of mass. Since the upper plate is permeable, the boundary conditions that have to be respected on Γ_{T} at all times are:

$$\wp(L,t) = 0, \tag{50a}$$

$$-\wp(L,t) + P_{\mathrm{sc}}^{zZ}(L,t) = P_{\mathrm{b}}(t) = \frac{\mathfrak{f}(t)}{\pi R_{\mathrm{c}}^2} \;\Rightarrow\; P_{\mathrm{sc}}^{zZ}(L,t) = P_{\mathrm{b}}(t). \tag{50b}$$

Since the lateral wall and the lower plate of the apparatus are fixed, rigid and impermeable, the radial displacement of the specimen and the radial component of the filtration velocity must vanish on Γ_{L}. Similarly, the axial displacement and the axial component of the filtration velocity must be zero on Γ_{B}. These conditions must apply at all times. The form of the deformation and pressure specified in (43a)–(43d) satisfies automatically the zero-displacement and no-flow conditions on Γ_{L}. However, to comply

with the requirements on the lower plate, ζ and $\wp$ must respect at all times the following boundary conditions on Γ_{B}:

$$\zeta(0,t) = 0\,, \tag{51a}$$

$$Q^Z(0,t) = 0 \;\Rightarrow\; \wp'(0,t) = 0\,. \tag{51b}$$

For the sake of rigour, we recall that the no-flux condition $Q^Z = 0$ is equivalent to $\wp' = 0$ only when no compaction occurs, i.e. for non-zero hydraulic conductivity (the friction factor f is always different from zero). Compaction is reached when J equals its lower bound $J = \phi_{\mathrm{sR}}$. In this case, k_0 is zero (cf. (31)). We remark, however, that compaction is never reached in the forthcoming results.

5.3 Solution strategy

It is important to notice that, due to (48b), the pressure gradient $\wp'$ can be expressed as a function of J and its partial derivative with respect to the axial coordinate, J', i.e.

$$\wp' = \frac{\partial P_{\mathrm{sc}}^{zZ}}{\partial Z} = \frac{\partial \hat{P}_{\mathrm{sc}}^{zZ}}{\partial J}(J)J'\,. \tag{52}$$

Hence, the friction factor f can be rephrased as $f = \hat{f}(J,\wp') \equiv \tilde{f}(J,J')$, cf. (27) and (47). This result allows to condense the set of equations (48a) and (48b) into the single, scalar, partial differential equation in the unknown J:

$$\dot{J} = \frac{\partial}{\partial Z}\left(\frac{f k_0}{J}\frac{\partial P_{\mathrm{sc}}^{zZ}}{\partial Z}\right) = \frac{\partial}{\partial Z}\left(\frac{\tilde{f}(J,J')\hat{k}_0(J)}{J}\frac{\partial \hat{P}_{\mathrm{sc}}^{zZ}}{\partial J}(J)J'\right)\,, \tag{53}$$

which has to be solved jointly with the boundary conditions

$$\frac{\partial \hat{P}_{\mathrm{sc}}^{zZ}}{\partial J}(J)J' = 0\,, \qquad \text{on } \Gamma_{\mathrm{B}}\,, \tag{54a}$$

$$\hat{P}_{\mathrm{sc}}^{zZ}(J) = \frac{H_{\mathrm{m}}}{2}\frac{J^2-1}{J^{2b+1}}\exp\{b[J^2-1]\} = P_{\mathrm{b}}(t)\,, \qquad \text{on } \Gamma_{\mathrm{T}}\,. \tag{54b}$$

Equations (54a) and (54b) are a rewriting of (51b) and (50b), respectively. The former one makes use of the identity (52), evaluated at $Z = 0$. Equation (54b), instead, is a non-linear Dirichlet boundary condition on J. Its fulfilment requires an iterative linearisation method, at each time step. Equation (53) can be regarded as a highly non-linear diffusion equation in the

volumetric ratio, in which

$$\mathcal{D} = \hat{\mathcal{D}}(J, J') := \frac{\tilde{f}(J, J')\hat{k}_0(J)}{J} \frac{\partial \hat{P}_{\rm sc}^{zZ}}{\partial J}(J) \tag{55}$$

plays the role of a non-linear diffusion coefficient depending on J and its derivative J'. A similar result has been recently discussed in [25, 26], in which, however, only Darcy's law was considered. The main difference between $\mathcal{D}$ in (55) and the diffusion coefficient obtained in [25, 26] is that $\mathcal{D}$ depends also on the derivative of the volumetric ratio. This is a consequence of the Forchheimer's correction that does not arise in the Darcian case.

Once J is computed, the axial deformation ζ and pressure $\wp$ can be determined *a posteriori* by invoking (51a), (50a) and (50b):

$$\zeta'(Z,t) = J(Z,t) \qquad \Rightarrow\ \zeta(Z,t) = \int_0^Z J(Y,t)\mathrm{d}Y\,, \tag{56a}$$

$$\frac{\partial \wp}{\partial Z} = \frac{\partial P_{\rm sc}^{zZ}}{\partial Z} \qquad \Rightarrow\ \wp(Z,t) = P_{\rm sc}^{zZ}(Z,t) - P_{\rm b}(t)\,. \tag{56b}$$

6 Numerics

The particularly simple form of the problem (53), along with the boundary conditions (54a) and (54b), and the initial condition $J(Z,0) = 1$, makes it convenient to search for solutions by employing Finite Difference schemes. The spatial discretisation of the interval $[0, L]$ is performed via the partition $0 = Z_1 < Z_2 < \ldots < Z_j < \ldots < Z_M = L$. For simplicity, the size of the spatial grid, $\Delta = Z_{j+1} - Z_j = L/M > 0$, is assumed to be constant for all $j = 1, \ldots, M-1$, so that $(M-1)$ subintervals $[Z_j, Z_{j+1}]$ of equal length are determined. For the discretisation in space of (53), we adapted to the problem at hand the second-order Finite Difference scheme used in [25, 26] for the purely Darcian case. Indeed, the introduction of the Forchheimer's correction necessitates the numerical evaluation of the friction factor, which, at each time step, requires to compute the Darcy's filtration velocity before computing J at the subsequent time instant. To this end, we used the following first-order discrete scheme, for $j = 2, \ldots, M$,

$$\begin{aligned} Q_{\rm D}^{Z}(Z_j,t) &= -\frac{k_0(Z_j,t)}{J(Z_j,t)} \left(\frac{\wp(Z_j,t) - \wp(Z_{j-1},t)}{\Delta} \right) \\ &= -\frac{k_0(Z_j,t)}{J(Z_j,t)} \left(\frac{P_{\rm sc}^{zZ}(Z_j,t) - P_{\rm sc}^{zZ}(Z_{j-1},t)}{\Delta} \right). \end{aligned} \tag{57}$$

We remark that, in (57), the space discrete version of (46), for $f = 1$, has been used. With $Q_{\mathrm{D}}^{Z}(Z_j, t)$, and the corresponding hydraulic conductivity $k_0(Z_j, t)$, one can compute the friction factor $f(Z_j, t)$, and solve the following set of ordinary differential equations in time

$$\begin{aligned}\dot{J}(Z_j,t) =& \frac{1}{\Delta^2}\left[\frac{f(Z_{j+1},t)k_0(Z_{j+1},t)}{J(Z_{j+1},t)}\left(P_{\mathrm{sc}}^{zZ}(Z_{j+1},t) - P_{\mathrm{sc}}^{zZ}(Z_j,t)\right)\right. \\ &\left. - \frac{f(Z_j,t)k_0(Z_j,t)}{J(Z_j,t)}\left(P_{\mathrm{sc}}^{zZ}(Z_j,t) - P_{\mathrm{sc}}^{zZ}(Z_{j-1},t)\right)\right],\end{aligned} \tag{58}$$

in which $j = 2, \ldots, (M-1)$ enumerates all the internal points of the interval $[0, L]$. The boundary conditions (54a) and (54b) are discretised as

$$\frac{J(Z_2,t) - J(Z_0,t)}{2\Delta} = 0\,, \tag{59a}$$

$$\frac{H_{\mathrm{m}}}{2}\frac{J(Z_M,t)^2 - 1}{J(Z_M,t)^{2b+1}}\exp\{b[J(Z_M,t)^2 - 1]\} = P_{\mathrm{b}}(t)\,, \tag{59b}$$

where Z_0 is a fictitious node introduced to approximate the zero-Neumann condition (54a). Equation (59b) is a non-linear Dirichlet boundary condition, which has to be satisfied at all times by $J(Z_M, t)$. For this purpose, we used a Newton-Raphson procedure.

Table 2: Parameters used in the simulations.

b	1.105 [36]
H_{m}	$0.407 \cdot 10^6$ MPa
L	$2 \cdot 10^{-3}$ m
m_0	0.0848
m_1	4.638
R_{c}	$2.5 \cdot 10^{-3}$ m
T_{end}	100 s
T_{ramp}	10 s
γ	0.2 kg
μ	$2 \cdot 10^{-3}$ Pa · s
ϕ_{sR}	0.2
ϱ_{f}	1000 kg/m^3

The set of ordinary differential equations given in (58) is discretised in time by means of a Backward Differentiation Formula (BDF), which can

arrive up to the fifth order. To solve (58), we chose a stiff Matlab® solver (ode15s). All the numerical parameters used in the numerical simulations are reported in table 2.

7 Results and discussion

In table 3, we report the values of each β-factor, which has been obtained by setting $k_{0\mathrm{R}} = 1 \cdot 10^{-15}$ m^4/(Ns). In table 4, instead, we report the results obtained by choosing $k_{0\mathrm{R}} = 1 \cdot 10^{-13}$ m^4/(Ns). These results are obtained by averaging β and f both in space and in time.

Table 3: Mean values in time and space of β and f, computed for $k_{0\mathrm{R}} = 1 \cdot 10^{-15}$ m^4/(Ns), i.e. $\langle\beta\rangle = \frac{1}{T_{\mathrm{end}}} \int_0^{T_{\mathrm{end}}} \left(\frac{1}{L} \int_0^L \beta(Z,t) \mathrm{d}Z \right) \mathrm{d}t$ and $\langle f\rangle = \frac{1}{T_{\mathrm{end}}} \int_0^{T_{\mathrm{end}}} \left(\frac{1}{L} \int_0^L f(Z,t) \mathrm{d}Z \right) \mathrm{d}t$.

β	$\langle\beta\rangle$ m^{-1}	$\langle f\rangle$
β_{TM}	$6.79 \cdot 10^{11}$	≈ 1
β_{JK}	$1.01 \cdot 10^{16}$	0.9997
β_{T}	$5.69 \cdot 10^{17}$	0.9866
β_{E}	$2.33 \cdot 10^{7}$	≈ 1
β_{G}	$3.72 \cdot 10^{8}$	≈ 1
β_{P}	$8.19 \cdot 10^{19}$	0.9073
β_{Li}	$7.54 \cdot 10^{14}$	≈ 1
β_{J}	$1.41 \cdot 10^{20}$	0.9028
β_{CH}	$2.03 \cdot 10^{23}$	0.8659
β_{A}	$4.44 \cdot 10^{15}$	≈ 1

The factors β_{TM}, β_{G}, β_{E}, β_{Li}, β_{A} that are smaller than the threshold value $\beta_{\mathrm{th}} = 1 \cdot 10^{16}$ 1/m, are not expected to produce relevant results.

The order of magnitude of the friction factor f is related to those quantities of the model that come into play in its definition (mainly the Darcy's filtration velocity $\boldsymbol{q}_{\mathrm{D}}$ and the hydraulic conductivity k_{eq}). To have a relevance in the model, the β-factor must balance both filtration velocity and hydraulic conductivity in such a way that smaller permeabilities should be balanced by higher β. Conversely, for instance, for higher flow rates (i.e. $\|\boldsymbol{q}_{\mathrm{D}}\| = O(10^{-5})$ m/s), even a smaller β can be weighty.

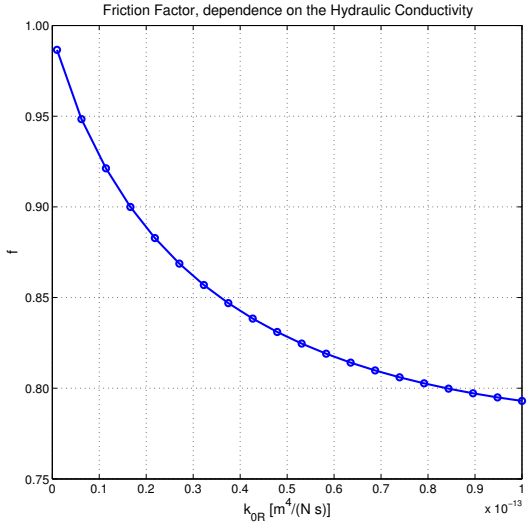

(a)

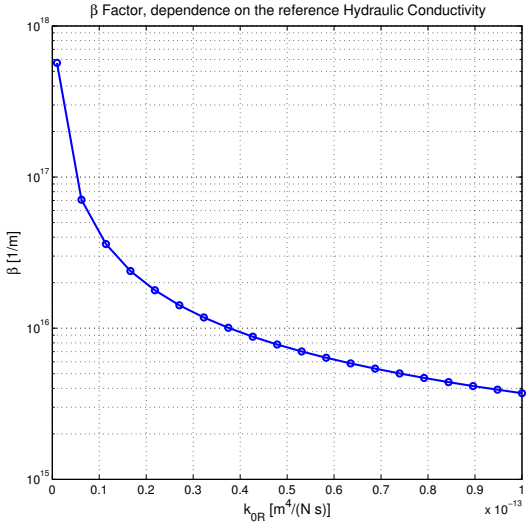

(b)

Figure 1: (a) Mean (in time and space) friction factor variation with $k_{0\mathrm{R}}$. (b) Mean (in time and space) variation (semi-logarithmic scale) of β_{T} with $k_{0\mathrm{R}}$.

By comparing table 3 with table 4, another peculiarity of the model can be observed. Namely, although the mean value of β diminishes with increasing k_{eq}, i.e. with increasing $k_{0\mathrm{R}}$, the friction factor f also diminishes, thereby supplying a greater contribution of the Forchheimer's correction to the model. This seems to be a contradiction with what stated above, when we wrote that the β-factors below the threshold value β_{th} do not contribute appreciably to the Forchheimer's correction. This apparent contradiction can be resolved by recalling that, beyond β, a key-role in the determination of f is also played by $k_{0\mathrm{R}}$ and $\|\boldsymbol{q}_{\mathrm{D}}\|$. Indeed, by increasing $k_{0\mathrm{R}}$, also $\|\boldsymbol{q}_{\mathrm{D}}\|$ increases, which lowers the value of the friction factor f. Therefore, we conclude that a delicate balance among all these quantities reveals how physically relevant the Forchheimer's correction is.

Table 4: Mean values in time and space of β and f, computed for $k_{0\mathrm{R}} = 1 \cdot 10^{-13}$ m^4/(Ns), i.e. $\langle\beta\rangle = \frac{1}{T_{\mathrm{end}}} \int_0^{T_{\mathrm{end}}} \left(\frac{1}{L} \int_0^L \beta(Z,t) \mathrm{d}Z \right) \mathrm{d}t$ and $\langle f\rangle = \frac{1}{T_{\mathrm{end}}} \int_0^{T_{\mathrm{end}}} \left(\frac{1}{L} \int_0^L f(Z,t) \mathrm{d}Z \right) \mathrm{d}t$.

β	$\langle\beta\rangle$ m^{-1}	$\langle f\rangle$
β_{TM}	$1.22 \cdot 10^{10}$	≈ 1
β_{JK}	$5.55 \cdot 10^{13}$	0.9955
β_{T}	$3.72 \cdot 10^{15}$	0.7930
β_{E}	$2.27 \cdot 10^{6}$	≈ 1
β_{G}	$2.97 \cdot 10^{7}$	≈ 1
β_{P}	$4.17 \cdot 10^{17}$	0.3321
β_{Li}	$1.13 \cdot 10^{14}$	0.9991
β_{J}	$1.47 \cdot 10^{17}$	0.3755
β_{CH}	$3.68 \cdot 10^{19}$	0.2847
β_{A}	$1.34 \cdot 10^{14}$	0.9890

In the following, we shall mainly refer to Tek's formula $\beta = \beta_{\mathrm{T}}$. As it can be deduced from tables 3 and 4, β_{T} is one of those that confirm the difference between the Darcy's model and the Forchheimer's one, although it is not the one that is expected to give the most significant influence of the Forchheimer's correction to the flow.

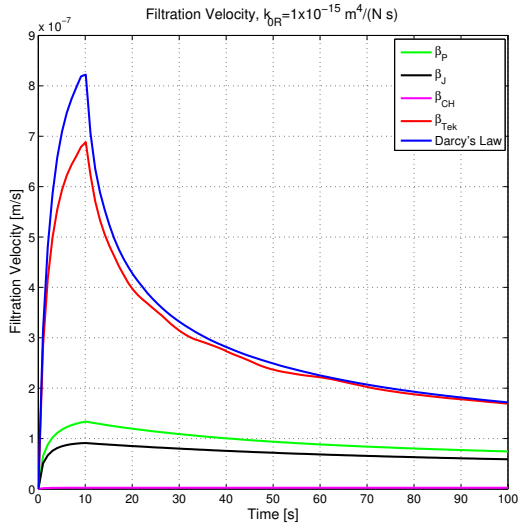

(a)

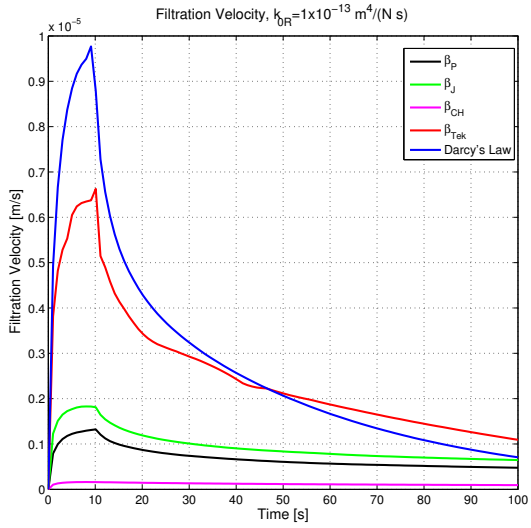

(b)

Figure 2: Filtration velocity vs time at the upper boundary of the computational domain for $k_{0\mathrm{R}} = 1 \cdot 10^{-15}$ m^4/(Ns) (a) and $k_{0\mathrm{R}} = 1 \cdot 10^{-13}$ m^4/(Ns) (b).

Figures 1(a) and 1(b) show, respectively, the variation of the friction factor f and the corresponding β-factor as a function of the reference hydraulic conductivity $k_{0\mathrm{R}}$. We notice that both f and β decrease with increasing $k_{0\mathrm{R}}$. In particular, the decrease of f leads to a stronger influence of the Forchheimer's correction on the flow.

In Figures 2(a) and 2(b), we report the trend of the filtration velocity at the upper boundary of the computational domain (i.e. at the surface through which the fluid escapes from the specimen) for the reference hydraulic conductivities $k_{0\mathrm{R}} = 1 \cdot 10^{-15}$ m^4/(Ns) and $k_{0\mathrm{R}} = 1 \cdot 10^{-13}$ m^4/(Ns), respectively. The filtration velocity grows with increasing $k_{0\mathrm{R}}$, as expected.

Another effect related to the introduction of the Forchheimer's correction is given by an increase of the characteristic time needed by the system to approach the stationary state, i.e. the state in which $\dot{J} = 0$. Indeed, the Darcy's filtration velocity decreases more steeply than that computed by means of the Forchheimer's correction (see Figures 2(a) and 2(b)). This result is independent of the choice of β. However, the curves of the filtration velocities corresponding to β_{P}, β_{J} and β_{CH} remain below the Darcy's curve for the all duration of the simulation, whereas the curve corresponding to β_{T} "touches" the Darcy's curve for $k_{0\mathrm{R}} = 1 \cdot 10^{-15}$ m^4/(Ns), and intersects it at about one half of the observation time ($T_{\mathrm{end}} = 100$ s) for $k_{0\mathrm{R}} = 1 \cdot 10^{-13}$ m^4/(Ns).

Looking at (53), we note that the stationary state is achieved when the pressure tends to zero at all points of the sample, or equivalently, when the stress P_{sc}^{zZ} becomes uniform along the specimen and tends pointwise to be equal to the applied load. Within the constitutive framework adopted in this paper, this result leads to a uniform distribution of the volumetric ratio J along the specimen, as shown in Figure 3.

In Figures 3(a) and 3(b), we show the spatial trend of P_{sc}^{zZ} and J at the end of the loading ramp, $t = 10$ s, and at the final instant of observation, $t = 100$ s, for both the Darcy's and the Forchheimer's case, respectively. The arrows indicate the direction of ascending hydraulic conductivity $k_{0\mathrm{R}}$. We notice that, at $t = 100$ s, increasing the hydraulic conductivity brings the system closer to its stationary state, as it is confirmed by the higher uniformity of the curves of stress and volumetric ratio reported in the right columns of Figures 3(a) and 3(b). It is important to remark that, at $t = 100$ s, the uniformity of the stress and volumetric ratio in the Darcy's

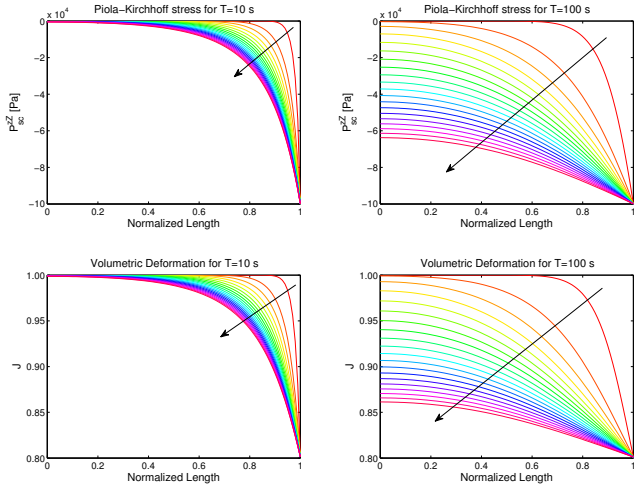

(a) Darcy-Forchheimer Law

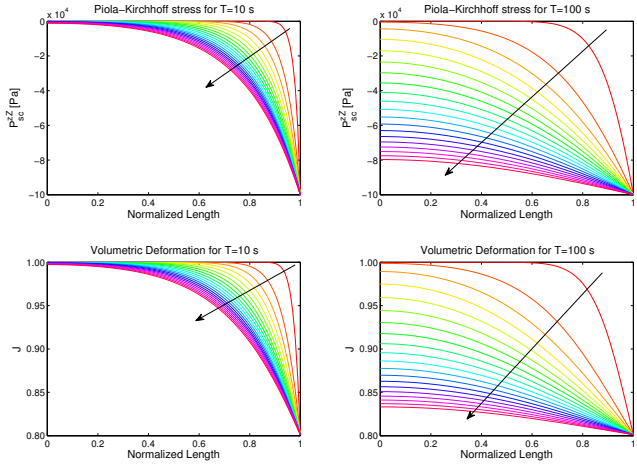

(b) Darcy's Law

Figure 3: (a) P_{sc}^{zZ} and J computed according to Darcy's law. (b) P_{sc}^{zZ} and J computed accounting for the Forchheimer's correction (with $\beta = \beta_{\mathrm{T}}$). The curves are evaluated at $t = 10$ s and $t = 100$ s. The arrows indicate the direction of ascending $k_{0\mathrm{R}}$.

model is more evident than that characterising the Forchheimer's one. Indeed, in the first ten seconds of the loading ramp, and with reference to the curves representing the Forchheimer's case, the main variations in space of $P_{\rm sc}^{zZ}$ and J remain confined to the upper part of the sample, while, in the Darcy's model, $P_{\rm sc}^{zZ}$ and J vary smoother in the whole sample with increasing $k_{0\rm R}$. At $t = 100$ s, and for the biggest value of the referential hydraulic conductivity, i.e. $k_{0\rm R} = 1 \cdot 10^{-13}$ m^4/(Ns), we obtain $P_{\rm sc}^{zZ}(0, 100) \approx -8 \cdot 10^4$ Pa in the Darcy's case, and $P_{\rm sc}^{zZ}(0, 100) \approx -6 \cdot 10^4$ Pa in the Forchheimer's case. Furthermore, at the same instant of time and for the same $k_{0\rm R}$, we find that J is slightly smaller than 0.84 in the Darcy's case, and approximately equal to 0.86 in the Forchheimer's one.

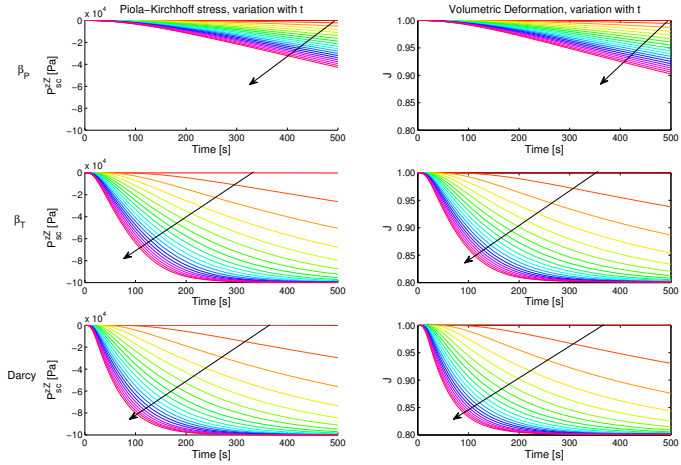

Figure 4: Time variation of $P_{\rm sc}^{zZ}$ (left) and J (right) at $Z = 0$. The arrows indicate the direction of ascending $k_{0\rm R}$.

In Figure 4, we show the time behaviour of $P_{\rm sc}^{zZ}$ and J. Each curve has been evaluated at the same point $Z = 0$, for different values of $k_{0\rm R}$. To observe the difference with which both $P_{\rm sc}^{zZ}$ and J approach the corresponding stationary solutions, we chose $T_{\rm end} = 500$ s for these simulations. Our results demonstrate that the Forchheimer's correction has the effect of diminishing the rapidity with which the system tends to the stationary state. In particular, keeping in mind that the Pascal factor $\beta_{\rm P}$ is one of the biggest factors in Table 4, we notice that the system, for $\beta = \beta_{\rm P}$ (see first row of

Figure 4), approaches the stationary state too slowly. Indeed, the interval of time over which the curve P_{sc}^{zZ} versus time is concave is much longer than in the other two cases (i.e. in the pure Darcy's case and in the Forchheimer's model with $\beta = \beta_{\mathrm{T}}$).

In all the results reported so far, we considered a homogeneous permeability model. If we switch to an inhomogeneous model [59], the Forchheimer's contribution becomes higher.

In Figure 5(b), we see that the filtration velocity obtained in the case of the inhomogeneous (depth-dependent) permeability model is always greater than the one obtained with a constant $k_{0\mathrm{R}}$. In the latter case, the friction factor (see Figure 5(a)) is higher than the one obtained in the first case.

8 Conclusions

In this work, we used the Darcy-Forchheimer law to describe fluid flow in a sample of articular cartilage undergoing a confined compression test, and modelled as a biphasic, solid-fluid mixture. The Forchheimer's correction is reflected by the friction factor f, which relates the Darcy's filtration velocity, $\boldsymbol{q}_{\mathrm{D}}$, to the filtration velocity $\boldsymbol{q}$ obtained within a second-order approximation of the solid-fluid interactions (cf. (24)). This approximation accounts for pore scale inertial effects [10]. Since f is strictly greater then zero and smaller than —or at most equal to— one, the magnitude of the filtration velocity computed by means of the Darcy-Forchheimer law, $\|\boldsymbol{q}\|$, is always a proper fraction of $\|\boldsymbol{q}_{\mathrm{D}}\|$.

In some of our numerical simulations, the Forchheimer's correction affects significantly the behaviour of the whole solid-fluid system by influencing the filtration velocity, pressure, constitutive stress and volumetric ratio. For example, for all those β factors that produced significant results, the magnitude of the filtration velocity was reduced of a percentage depending on the value of f, and the peak attained at the end of the loading ramp (see Figures 2(a) and 5(b)) was smaller than that obtained by using Darcy's law. Moreover, when the effect of the Forchheimer's correction was strong enough, the pressure computed by using the Forchheimer's correction was higher than that predicted by Darcy's law and, consequently, the solid-fluid system reached the stationary state more slowly than in the pure Darcian case. Indeed, since the pressure must be zero at the stationary state (this is, indeed, the only constant solution to (48a) that complies with the boundary condition $\wp(L,t) = 0$), higher pressures necessitate longer time to vanish at

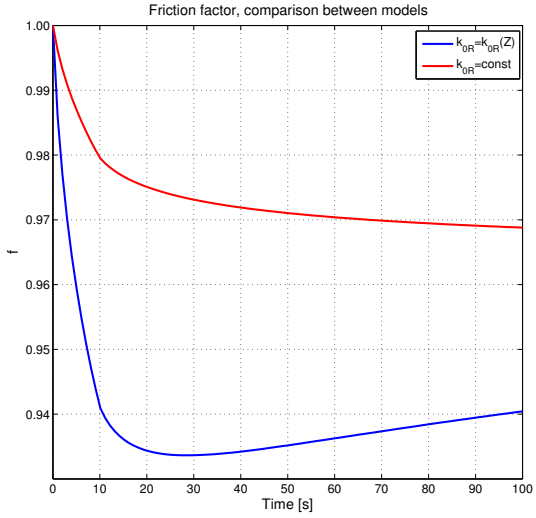

(a)

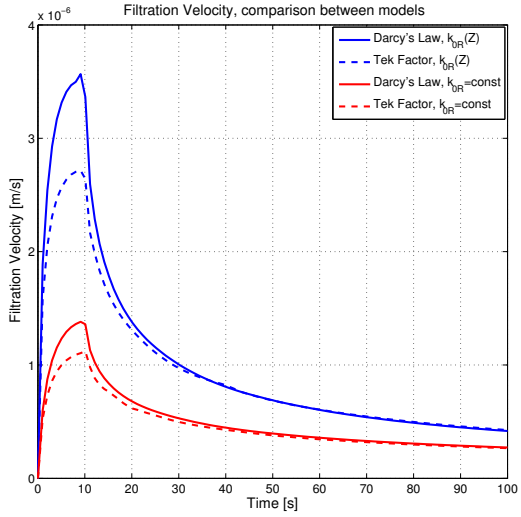

(b)

Figure 5: (a) Space average $\langle f \rangle$ for the depth-dependent hydraulic conductivity model and for the constant hydraulic conductivity model. (b) Filtration velocities vs time for the Darcy's case and the Forchheimer's case, with $\beta = \beta_{\mathrm{T}}$, for the inhomogeneous and the homogeneous hydraulic conductivity models.

all points of the sample.

According to our calculations, the effectiveness of the Forchheimer's correction depends substantially on $k_{0\mathrm{R}}$, β, and the magnitude of the pressure gradient. Indeed, since the influence of the Forchheimer's correction becomes stronger when f diminishes, and since f is a decreasing function of $k_{0\mathrm{R}}$, β and $|\wp'|$, increasing one of these quantities (or the three of them) turns into a more evident deviation of our results from those predicted by the standard Darcy's law. To emphasise this fact, we notice that, looking at (47), the efficacy of the Forchheimer's correction is related to the term

$$4A\frac{k_0|\wp'|}{J} = 4\varrho_{\mathrm{f}}\beta(k_{0\mathrm{R}})^2|\wp'|\frac{1}{J}\left(\frac{J-\phi_{\mathrm{sR}}}{1-\phi_{\mathrm{sR}}}\right)^{2m_0}\exp\left[m_1(J^2-1)\right] .$$

This confirms that $k_{0\mathrm{R}}$, β and $|\wp'|$ are the parameters which one has to play with, and shows that β and $|\wp'|$ should compensate for the smallness of $(k_{0\mathrm{R}})^2$, which —in some of the cases studied in this paper— has order of magnitude 10^{-30} $\mathrm{m}^4/(\mathrm{Ns})$. We visualised this behaviour by running numerical simulations for different values of $k_{0\mathrm{R}}$, which ranged between $k_{0\mathrm{R}} = 1\cdot10^{-15}$ $\mathrm{m}^4/(\mathrm{Ns})$ and $k_{0\mathrm{R}} = 1\cdot10^{-13}$ $\mathrm{m}^4/(\mathrm{Ns})$. The smallest value has the same order of magnitude as the one in [36]. The biggest value, instead, is one order of magnitude smaller than the experimental data reported in [11], in which the mean hydraulic conductivity reaches $\bar{k}_{0\mathrm{R}} = 1.3\cdot10^{-12}$ $\mathrm{m}^4/(\mathrm{Ns})$, a value referring to the superficial layers of articular cartilage. To discuss the role of the pressure gradient, we recall that the most recurrent applications of non-linear constitutive laws for $\boldsymbol{m}_{\mathrm{fd}}$, i.e. the dissipative part of the momentum exchange rate, are the ones in which a fluid flows at relatively high velocity through the matrix of a porous medium. For fixed values of the referential hydraulic conductivity, these situations require high pressure gradients. In these cases, the corresponding friction factors can be sufficiently smaller than one, thereby leading to effective Forchheimer's corrections, even for rather small β-factors. Finally, we remark that, by raising $k_{0\mathrm{R}}$, both f and β decrease. However, while the diminishing of f plays in favour of the Forchheimer's correction, the diminishing of β plays against it. For small values of $k_{0\mathrm{R}}$, the predominant contribution to the Forchheimer's correction is given by the β-factor, while, for big values of $k_{0\mathrm{R}}$, the magnitude of the pressure gradient prevails.

Finally, we studied the effect of the inhomogeneity of the hydraulic conductivity on the strength of the Forchheimer's correction. For this purpose, we used the model presented in [59], where a depth-dependent hydraulic

conductivity is considered, and compared the results with those obtained by employing a homogeneous hydraulic conductivity. We found that adopting a depth-dependent hydraulic conductivity enhances the effectiveness of the Forchheimer's correction for all the chosen values of $k_{0\mathrm{R}}$ and independently on the order of magnitude of the filtration velocity.

A comparison of the results discussed in this paper with experimental data available in the literature should be done in order to choose —or to fit— β-factors with a clearer biomechanical meaning, to determine their ranges of variation, e.g., with the age and health of a real sample of tissue, and to investigate in more detail the true physical relevance of the Forchheimer's correction in modelling articular cartilage.

The study done in this work ought to be generalised to consider the presence of collagen fibres, along with their influence on both the elastic and the hydraulic properties of articular cartilage. A possible way of pursuing this goal is the inclusion of the Forchheimer's correction into the anisotropic and inhomogeneous model of articular cartilage recently presented in [59]. This could be useful to assess the interplay between the tissue's structural anisotropy, which supplies guidance to the flow due to the presence of the collagen fibres, and the non-linearities arising from a better approximation of the fluid filtration velocity. Moreover, it could be interesting to consider also the presence of growth and remodelling [2, 3, 22–24, 28, 29].

Acknowledgments

AG would like to warmly thank his wife and children for their patience and love. SF would like to acknowledge the support of Alberta Innovates - Technology Futures (Canada), through the AITF New Faculty Programme, Alberta Innovates - Health Solutions (Canada), through the Sustainability Programme, and the Natural Sciences and Engineering Research Council of Canada, through the NSERC Discovery Programme.

Nomenclature

Latin symbols	**Description**
A	Forchheimer's coefficient
b	Material parameter of the Holmes-Mow strain energy
c_i	Parameters defining the β-factor ($i = 1, 2, 3$)
$\boldsymbol{C}$	Right Cauchy-Green deformation tensor
$\mathcal{C}_{\mathrm{R}}$, $\mathcal{C}_t$	Reference and current configurations
f	Friction factor
$\mathfrak{f}$	Applied load
$\mathfrak{f}_{\max}$	Maximum applied load
H_{m}	Aggregate axial modulus
$\boldsymbol{H}$	Material pressure gradient
I_i	Invariants of $\boldsymbol{C}$ ($i = 1, 2, 3$)
$\mathfrak{I}_4$	Invariant-like quantity defined in (26)
$\boldsymbol{k}$	Spatial hydraulic conductivity
k_0	Scalar hydraulic conductivity
k_{eq}	Equivalent hydraulic conductivity
$k_{0\mathrm{R}}$	Referential hydraulic conductivity
$\boldsymbol{K}$	Material hydraulic conductivity
$\ell(t)$	Height of the deformed specimen at time t
L	Height of the undeformed specimen
m_0, m_1	Parameters characterising the hydraulic conductivity
$\boldsymbol{m}_\alpha$	Momentum exchange rate of the α-th phase ($\alpha = \mathrm{f}, \mathrm{s}$)
$\boldsymbol{m}_{\mathrm{fd}}$	Dissipative part of $\boldsymbol{m}_{\mathrm{f}}$
p	Pore pressure
$\boldsymbol{P}_\alpha$	First Piola-Kirchhoff stress of the α-th phase ($\alpha = \mathrm{f}, \mathrm{s}$)
$\boldsymbol{P}_{\mathrm{sc}}$	Constitutive part of $\boldsymbol{P}_{\mathrm{s}}$
$\wp$	Pore pressure as a function of the axial coordinate
$\boldsymbol{q}$	Darcy-Forchheimer's filtration velocity
$\boldsymbol{q}_{\mathrm{D}}$	Darcy's filtration velocity
$\boldsymbol{Q}$	Material Darcy-Forchheimer's filtration velocity
$\boldsymbol{Q}_{\mathrm{D}}$	Material Darcy's filtration velocity
$\boldsymbol{r}$	Resistivity of the porous medium
R_{c}	Radius of the undeformed specimen
T_{end}	Final time of the simulation
T_{ramp}	End of the loading ramp

$\boldsymbol{v}_\alpha$	Velocity of the α-th phase ($\alpha = \mathrm{f}, \mathrm{s}$)
$\hat{W}$	Strain energy density of the solid phase

Greek symbols	**Description**
α_0, α_1, α_2	Material parameters of the Holmes-Mow strain energy
β	β-factor
γ	Proportionality constant of the load
Γ_B, Γ_L, Γ_T	Bottom, top and lateral boundaries of the specimen
ζ	Displacement as a function of the axial coordinate
κ_0	Scalar permeability
κ_eff	Effective permeability
$\boldsymbol{\kappa}$	Permeability
μ	Dynamic viscosity of the fluid
ϱ_α	True mass density of the α-th phase, $\alpha = \mathrm{f}, \mathrm{s}$
$\boldsymbol{\sigma}_\alpha$	Cauchy stress tensor of the α-th phase
$\boldsymbol{\sigma}_\mathrm{sc}$	Constitutive part of $\boldsymbol{\sigma}_\mathrm{s}$
τ	Tortuosity
ϕ_α	Volumetric fraction of the α-th phase ($\alpha = \mathrm{f}, \mathrm{s}$)
ϕ_sR	Piola transform of ϕ_s, i.e. $\phi_\mathrm{sR} = J\phi_\mathrm{s}$
χ	Motion of the solid phase

References

[1] Aminian, K., Ameri, S., Yussefabad, A.G., A simple and reliable method for gas well deliverability determination, SPE-111195-MS, SPE Eastern Regional Conference in Lexington, Kentucky, USA (2007).

[2] Andreaus, U., Giorgio, I., Lekszycki, T., A 2-D continuum model of a mixture of bone tissue and bio-resorbable material for simulating mass density redistribution under load slowly variable in time, *ZAMM - Zeitschrift für Angewandte Mathematik und Mechanik / Journal of Applied Mathematics and Mechanics*, 94 (2014), 12, pp. 978–100

[3] Andreaus, U., Giorgio, I., Madeo, A., Modeling of the interaction between bone tissue and resorbable biomaterial as linear elastic materials with voids, *ZAMP - Zeitschrift für Angewandte Mathematik und Physik / Journal of Applied Mathematics and Physics*, 66 (2015), pp. 209–237.

[4] Aspden, R.M., Hukins, D.W.L., Collagen organization in articular cartilage, determined by X-ray diffraction, and its relationship to tissue function, *Proc. R. Soc. B*, 212 (1981), pp. 299–304.

[5] Athanasiou, K.A., Rosenwasser, M.P., Buckwalter, J.A., Malinin, T.I., Mow, V.C., Interspecies comparisons of in situ intrinsic mechanical properties of distal femoral cartilage. *J. Orthopaedic Res.*, 9 (1991), pp. 330–340.

[6] Ateshian, G.A., On the theory of reactive mixtures for modeling biological growth. *Biomech. Model. Mechanobiolg.*, 6 (2007), 6, pp. 423–445.

[7] Ateshian, G.A., Weiss, J.A., Anisotropic Hydraulic Permeability Under Finite Deformation. *J. Biomech. Eng.*, 132 (2010), pp. 111004-1–111004-7.

[8] Bear, J, Bachmat, Y., *Introduction to modeling of transport phenomena in Porous Media*, Kluwer, Dordrecht, Boston, London, 1990.

[9] Bennethum, L.S., Murad, M.A., Cushman, J.H., Macroscale thermodynamics and the chemical potential for swelling porous media, *Transp. Porous Media*, 39 (2000), pp. 187–225.

[10] Bennethum, L.S., Giorgi, T., Generalized Forchheimer equation for two-phase flow based on hybrid mixture theory, *Transp. Porous Media*, 26 (1997), pp. 261–275.

[11] Boschetti, F., Pennati, G., Gervaso, F., Peretti, G.M., Biomechanical properties of human articular cartilage under compressive loads, *Biorheology*, 41 (2004), pp. 159–166.

[12] Chukwudozie, C.P., Tyagi, M., Sears, S.O., White, C.D., Prediction of non-Darcy coefficients for inertial flows through the Castlegate Sandstone using image-based modeling, *Transp. Porous Med.*, 95 (2012), pp. 563–580.

[13] Coles, M.E., Hartman, K.J., Non-Darcy Measurements in Dry Core and the Effect of Immobile Liquid. SPE-39977-MS, SPE Gas Technology Symposium, 15–18 March, Calgary, Alberta, Canada, p. 193. (1998).

[14] dell'Isola, F., Madeo, A., Seppecher, P., Boundary conditions at fluid-permeable interfaces in porous media: A variational approach, *Int. J. Solids. Struct.*, 46 (2009), 17, pp. 3150–3164.

[15] dell'Isola, F., Steigmann, D., A two-dimensional gradient-elasticity theory for woven fabrics, *Journal of Elasticity*, 118 (2015), 1, pp. 113–125.

[16] Ergun, S., Fluid Flow through Packed Column. *Chem. Eng. Prog.*, 48 No.2 (1952), pp. 89–94.

[17] Federico, S., Grillo, A., Elasticity and permeability of porous fibre-reinforced materials under large deformations, *Mech. Mat.*, 44 (2012), pp. 58–71.

[18] Federico, S., Hezog, W., On the anisotropy and inhomogeneity of permeability in articular cartilage, *Biomech. Model. Mechanobiol.*, 7 (2008), pp. 367–378.

[19] Federico, S., Herzog, W., On the permeability of fibre-reinforced porous materials, *Int. J. Solids Struct.*, 45 (2008), pp. 2160–2172.

[20] Gasser, T.C., Ogden, R.W., Holzapfel, G.A., Hyperelastic modelling of arterial layers with distributed collagen fibre orientations, *J. R. Soc. Interface*, 3 (2006), 15–35.

[21] Geerstma, J., Estimating the coefficient of inertial resistance in fluid flow through porous media, *Society of Petroleum Engineering*, 14 (1974), 5, pp. 445–450

[22] Giorgio, I., Andreaus, U., Madeo, A., The influence of different loads on the remodeling process of a bone and bio-resorbable material mixture with voids, *Continuum Mechanics and Thermodynamics*, (2014), DOI: 10.1007/s00161-014-0397-y

[23] Grillo, A., Federico, S., Giaquinta, G., Herzog, W., La Rosa, G., Restoration of the symmetries broken by reversible growth in hyperelastic bodies, *Theoret.Appl.Mech. TEOPM7*, 30 (2003), 4, pp. 311–331.

[24] Grillo, A., Federico, S., Wittum, G., Growth, mass transfer, and remodeling in fiber-reinforced, multi-constituent materials, *Int. J. Non-Linear. Mech.*, 47 (2012), pp. 388–401.

[25] Grillo, A., Giverso, C., Favino, M., Krause, R., Lampe, M., Wittum, G., "Mass Transport in Porous Media with Variable Mass". In *Numerical Analysis of Heat and Mass Transfer in Porous Media—Advanced and Structural Materials*, J.M.P.Q. Delgado, A.G.B. de Lima, and M.V. da Silva, eds., Springer-Verlag, Berlin, Heidelberg, pp. 27–61.

[26] Grillo, A., Guaily, A., Giverso, C., Federico, S., Non-linear Model for Compression Tests on Articular Cartilage, *Submitted.*

[27] Grillo, A., Logashenko, D., Stichel, S., Wittum, G., Forchheimer's correction in modelling flow and transport in fractured porous media, *Comput Visual Sci*, 15 (2012), pp. 169–190.

[28] Grillo, A., Wittum, G., Tomic, A., Federico, S., Remodelling in statistically oriented fibre-reinforced materials and biological tissues, *Mathematics and Mechanics of Solids*, 10.1177/1081286513515265, In press.

[29] Grillo, A., Zingali, G., Borrello, D., Federico, S., Herzog, W., Giaquinta, G., A multiscale description of growth and transport in biological tissues, *Theoret.Appl.Mech. TEOPM7*, 34 (2007), 1, 51–87.

[30] Guilak, F., Ratcliffe, A., Mow, V.C., Chondrocyte deformation and local tissue straining articular cartilage: a confocal microscopy study, *J. Orthopaedic Res.*, 13 (1995), pp. 410–421.

[31] Hackl, K., Fischer, F.D., On the relation between the principle of maximum dissipation and inelastic evolution given by dissipation potentials, *Proc. R. Soc. Lond.*, A464, (2007), pp. 117–132.

[32] Hassanizadeh, S.M., Derivation of basic equations of mass transport in porous media, Part 1. Macroscopic balance laws, *Adv. Water Resources*, 9 (1986), pp. 196–206.

[33] Hassanizadeh, S.M., Derivation of basic equations of mass transport in porous media, Part 2. Generalized Darcy's and Fick's laws, *Adv. Water Resources*, 9 (1986), pp. 207–222.

[34] Hassanizadeh, S.M., Gray, W.G., High velocity flow in porous media, *Transp. in Porous Media*, 2 (1987), pp. 521–531.

[35] Hassanizadeh, S.M., Lejinse, A., A non-linear theory of high-concentration-gradient dispersion in porous media, *Adv. Water Resources*, 18 (1995), 4, pp. 203–215.

[36] Holmes, M.H., Mow, V.C., The nonlinear characteristics of soft gels and hydrated connective tissues in ultrafiltration, *J. Biomech.*, 23 (1990), pp. 1145–1156.

[37] Holzapfel, G.A., Gasser, T.C., Ogden, R.W., A new constitutive framework for arterial wall mechanics and a comparative study of material models, *J. Elast.*, 61 (2000), pp. 1–48.

[38] Janicek, J.D., Katz, D.L., *Application of Unsteady State Gas Flow Calculations*, Proc. of University of Michigan Research Conference, (1955).

[39] Jones, S.C., Using the inertial coefficient, B, to characterize heterogeneity in reservoir rock, SPE-16949-MS, SPE Annual Technical Conference and Exhibition, 27-30 September, Dallas, Texas, USA, p. 165 (1987).

[40] Lekszycki, T., dell'Isola, F., A mixture model with evolving mass densities for describing synthesis and resorption phenomena in bones reconstructed with bio-resorbable materials, *ZAMM - Zeitschrift für Angewandte Mathematik und Mechanik / Journal of Applied Mathematics and Mechanics*, 92 (2012), 6, pp. 426–444

[41] Li, L.P., Soulhat, J., Buschmann, M.D., Shirazi-Adl, A., Nonlinear analysis of cartilage in unconfined ramp compression using a fibril reinforced poroelastic model, *Clinical Biomechanics*, 14 (1999), pp. 673–682.

[42] Li, D., Engler, T.W., Literature review on correlations of non-Darcy coefficient. SPE-70015-MS, SPE Permian Basin Oil and Gas Recovery Conference, 15-17 May, Midland, Texas, USA (2001).

[43] Linn, F.C., Sokoloff, L., Movement and composition of interstitial fluid of cartilage, *Arth. Rheum.*, 8 (1965), pp. 481–494.

[44] Madeo, A., dell'Isola, F., Darve, F., A Continuum Model for Deformable, Second Gradient Porous Media Partially Saturated with Compressible Fluids, *Journal of the Mechanics and Physics of Solids*, 61 (2013), 11, pp. 2196–2211.

[45] Mansour, J.M., *Biomechanics of cartilage*, Chapter 5, pp. 66–67. In *Kinesiology: the mechanics and pathomechanics of human movement*, Oatis, C.A. (Ed.), Lippincott Williams & Wilkins, Philadelphia, 2003.

[46] Maroudas, A., Bullough, P., Permeability of articular cartilage, *Nature*, 219 (1968), pp. 1260–1261.

[47] Marsden, J.E., Hughes, T.J.R., *Mathematical Foundations of Elasticity*, Dover Publications, Inc., New York, 1983.

[48] Merodio, J., Ogden, R.W., Mechanical response of fiber-reinforced incompressible non-linearly elastic solids, *Int. J. Non-Linear Mech.*, 40 (2005), pp. 213–227.

[49] Mollenhauer, J., Aurich, M., Muehleman, C., Khelashvilli, G., Irving, T.C., X-ray diffraction of the molecular substructure of human articular cartilage, *Connective Tissue Res.*, 44 (2003), pp. 201–207.

[50] Mow, V.C., Holmes, M.H., Lai, W.M., Fluid transport and mechanical properties of articular cartilage: a review, *J. Biomech.*, 17 (1984), pp. 377–394.

[51] Pascal, H., Ronald, G., Kingston, D.J., Analysis of vertical fracture length and non-Darcy flow coefficient using variable rate tests, SPE-9348-MS, SPE Annual Technical Conference and Exhibition, 21-24 September, Dallas, Texas, USA (1980).

[52] Pierce, D.M., Ricken, T., Holzapfel, G.A., A hyperelastic biphasic fibre-reinforced model of articular cartilage considering distributed collagen fibre orientations: continuum basis, computational aspects and applications, *Comput. Meth. Biomech. Biomed. Eng.*, 16 (2013), pp.1344–1361.

[53] Placidi, L., dell'Isola, F., Ianiro, N., Sciarra, G., Variational formulation of pre-stressed solid-fluid mixture theory, with an application to wave phenomena, *European Journal of Mechanics, A/Solids*, 27 (2008), 4, pp. 582–606.

[54] Quiligotti, S., On bulk mechanics of solid-fluid mixtures: kinematics and invariance requirements, *Theoret.Appl.Mech. TEOPM7*, 28 (2002), pp. 1–11.

[55] Quiligotti, S., Maugin G.A., Dell'Isola, F., An Eshelbian approach to the nonlinear mechanics of constrained solid-fluid mixtures, *Acta Mech.*, 160 (2003), pp. 45–60.

[56] Ruth, D.W., Ma, H., On the derivation of the Forchheimer equation by means of the averaging theorem, *Transp. Porous Media*, 7 (1992), pp. 255–264.

[57] Tek, M.R., Coats, K.H., Katz, D.L,. The effect of turbulence on flow of natural gas through porous media, *Journal of Petroleum Engineering*, 14 (1962), 7, pp. 799-806.

[58] Thauvin, F., Mohanty, K.K., Network modeling of non-Darcy flow through porous media, *Transp. in Porous Media*, 31 (1998), 19–37.

[59] Tomic, A., Grillo, A., Federico, S., Poroelastic materials reinforced by statistically oriented fibres—numerical implementation and application to articular cartilage, *IMA J. Appl. Math.*, 79 (2014), 5, pp. 1027–1059.

[60] Whitaker, S., The Forchheimer equation: A theoretical development, *Transp. Porous Media*, 25 (1996), pp. 27–61.

List of Figures

List of Tables

Submitted in November 2014, revised in December 2014.

Darcy-Forchheimer-ov zakon za modeliranje fluidnog tečenja u biološkim tkivima

Kretanje intersticijalnog fluida nekog biološkog tkiva se proučava primenom Darcy-Forchheimer-ovog zakona, koji je popravka standardnog Darcy-jevog zakona. Tkivo se modelira kao zasićena dvofazna sredina koja sadrži fluid i deformabolnu matricu. Razlog za preduzimanje ovog proučavanja je da opis dinamike tkiva zasnovanog na Darcy-Forchheimer-ovom zakonu može da bude potpuniji nego onaj zasnovan na Darcy-jevom zakonu, jer ovaj prvi obezbedjuje bolju makroskopsku reprezentaciju mikroskopskog medjudejstva fluid-čvrsto telo. Numeričkim simulacijama analiziran je uticaj Forchheimer-ove popravke.

doi:10.2298/TAM1404281G Math.Subj.Class.: 74B20, 74D10, 74E05, 74E10, 74E30, 74F10.